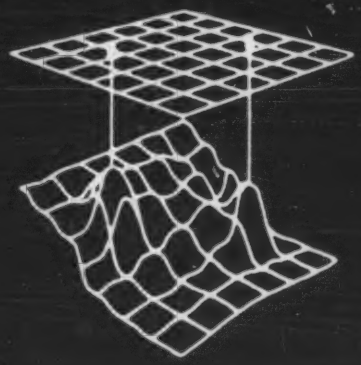

CMG CMG CMG CMG CMG

COMPUTER
MODELLING
GROUP

92-00207/

Part of Energy, Mines and Resources Cost-Shared Energy Conversion Program
and Part of the Program of the Federal Panel on Energy R&D (PERD)

FIELD-SCALE SIMULATION OF HORIZONTAL WELLS

Final Report by:

David Collins
Long Nghiem
Ravi Sharma
Yau-Kun Li
Dennis Coombe
Viera Oballa
Computer Modelling Group

Work on the project was conducted under the auspices of the Canada Centre for Mineral and Energy Technology, Energy, Mines and Resources Canada

DSS File No. 06SQ.23440-8-9237
DSS Contract Serial No. 23440-8-9237/01-SQ
CANMET Scientific Authority: Dr. Kamal Jha

March 31, 1990

55 pp

MICROMEDIA

ABSTRACT

A technique for the efficient modelling of horizontal wells in reservoir simulation is presented. This technique treats the horizontal well as a second "porosity" as in the dual-porosity approach for naturally fractured reservoirs. The well "permeability" and "relative permeabilities" are adjusted to yield the pressure drop and phase slip predicted from multiphase flow correlations. Because the wellbore flow equations are cast into the same form as the reservoir flow equations, efficient techniques that have been developed for reservoir simulation can readily be applied. The technique is developed for black-oil systems and extended to thermal systems. The use of elliptical grid refinement for improved predictions of flow phenomena around the wellbore is also presented.

Black-oil examples illustrating the application of the technique are given for the prediction of a horizontal well in a reservoir where water coning and gas cusping are important. As an example of the thermal application, a dual horizontal well (injector/producer) steam assisted gravity drainage process is modelled.

TABLE OF CONTENTS

	ABSTRACT	i
	TABLE OF CONTENTS	ii
	LIST OF TABLES	iii
	LIST OF FIGURES	iv
1.	INTRODUCTION	1-1
2.	WELLBORE FLOW EQUATIONS	2-1
	2.1 Outline	
	2.2 Single-Phase and Homogeneous Flow in Wellbore	
	2.3 Extension to Multiphase Flow With Slippage or Holdup	
	2.4 Wellbore Discretized Equations	
	2.5 An Alternate Approach: Integration of a Pressure-Drop Equation	
	2.6 Extension of Dual-Porosity Approach to Thermal Simulation	
3.	HYBRID GRID	3-1
	3.1 Outline	
	3.2 Elliptical Grid Refinement	
4.	EXAMPLE	4-1
	4.1 Outline	
	4.2 Light Oil Recovery From a Horizontal Well	
	4.3 Elliptical Grid Refinement	
	4.4 Steam Assisted Gravity Drainage	
5.	CONCLUSIONS	5-1
6.	NOMENCLATURE	6-1
7.	ACKNOWLEDGEMENT	7-1
8.	REFERENCES	8-1
9.	TABLES	9-1
10.	FIGURES	10-1

LIST OF TABLES

Table 1: Reservoir Cross Section and Initial Conditions

Table 2: Fluid Property Data

Table 3: Relative Permeabilities and Capillary Pressures

Table 4: Selected Simulation Parameters
Steam Assisted Gravity Drainage Process

LIST OF FIGURES

Figure 1: Reservoir Cross Sections with a Horizontal Well

Figure 2: Transformation of a Homogeneous, Anisotropic with a Circular Well to an Equivalent Homogeneous, Isotropic Reservoir

Figure 3: Elliptical Grid Refinement Around the Horizontal Well

Figure 4: Horizontal Producer in Layer 4

Figure 5: Water Cut and GOR Behavior for Horizontal Wells of Length 900 ft and 2100 ft with Liquid Rates of 3,000 Stb/day

Figure 6: Water Cut and GOR Behavior for Horizontal Wells of Length 900 ft and 2100 ft with Liquid Rates of 6,000 Stb/day

Figure 7: Oil Production Rates and Cumulative Oil Produced for Horizontal Wells of Length 900 ft and 2100 ft with Liquid Rates of 3,000 Stb/day

Figure 8: Oil Production Rates and Cumulative Oil Produced for Horizontal Wells of Length 900 ft and 2100 ft with Liquid Rates of 6,000 Stb/day

Figure 9: Water Production Rates and Cumulative Water Produced for Horizontal Wells of Length 900 ft and 2100 ft with Liquid Rates of 3,000 Stb/day

Figure 10: Water Production Rates and Cumulative Water Produced for Horizontal Wells of Length 900 ft and 2100 ft with Liquid Rates of 6,000 Stb/day

Figure 11: Gas Production Rates and Cumulative Gas Produced for Horizontal Wells of Length 900 ft and 2100 ft with Liquid Rates of 3,000 Stb/day

Figure 12: Gas Production Rates and Cumulative Gas Produced for Horizontal Wells of Length 900 ft and 2100 ft with Liquid Rates of 6,000 Stb/day

Figure 13: Variation of the Parameter α, the In Situ Gas Saturation (S_g) and the Correlation Predicted Gas Holdup (E_g) for the Wellblock Located in Gridblock (8,5,4). The Horizontal Well Length is 900 ft with a Liquid Rate of 6,000 Stb/day

Figure 14: Comparison of Water Cut and GOR for a Horizontal Well (Length = 2100 ft and Liquid Rate = 6,000 Stb/day) Modelled with No Grid Refinement and Using Hybrid Grid Refinement (4 Radial, 4 Tangential)

Figure 15: Predicted GOR for a Horizontal Well Modelled Using Different Levels of Hybrid Grid Refinement (Length = 2100 ft and Liquid Rate = 6,000 Stb/day)

Figure 16: A Comparison of Cumulative Oil Production Predictions Using Traditional Source/Sink vs. New Wellbore Model for a Thermal, Dual Horizontal Well, Gravity Drainage Example

Figure 17: A Comparison of Instantaneous Oil Production Predictions Using Traditional Source/Sink vs. New Wellbore Model for a Thermal, Dual Horizontal Well, Gravity Drainage Example

Figure 18: Gas Saturation Profile (Vertical y-z Cross Section, I=1) After 1825 Days, Showing Tangential (Slope) Growth of the Steam Chamber

1. INTRODUCTION

Recent interest in horizontal wells has been rapidly accelerating because of improved drilling technology, and the increased efficiency and economy of oil recovery operations. A recent report by Karisson and Bitto (1989) indicated that since the early 1980s, there have been more than 700 horizontal wells drilled with approximately 200 of those in 1988 alone.

The improvement in recovery and economics obtained with a horizontal well results from the extensive contact with the reservoir. This results in lower fluid velocities around the wellbore, while providing total flow rates which are economic. Typical applications of a horizontal well include:

- Reservoirs where conventional wells have low productivity; the use of horizontal drilling can be viewed as a method for well stimulation.

- Reservoirs where recovery is limited by water coning or gas cusping. This occurs usually when a thin oil column (approximately 15 m or 50 ft thick) is sandwiched between a gas cap and an aquifer. The use of horizontal wells in this case lowers the pressure gradient near the wellbore and therefore reduces the water coning and gas cusping tendencies while allowing an economic production rate.

- Reservoirs with vertical fractures. Horizontal drilling allows the intersection of many vertical fractures which form the main flow paths in the reservoir (Butler, 1988).

- Heavy-oil and tar-sands reservoirs where steam-assisted gravity drainage (SAGD) is practical. The process consists of injecting steam into an upper well and using a lower horizontal well as a producer to collect the draining oil and condensate from the steam chamber.

Since the drilling costs of horizontal wells are 1.4 to 4.0 times more than those of vertical wells, it is imperative to conduct a reservoir engineering study of the recovery economics of horizontal wells before drilling. A reservoir simulator with horizontal-well capabilities can provide guidance into the design of well lengths, locations, optimal flow rates to prevent water coning or gas cusping and can predict the increase in recovery over that of conventional wells.

One approach to the development of horizontal well capabilities in a reservoir simulator is to solve simultaneously the equations of conservation of mass, momentum and energy in the horizontal wellbore together with the reservoir equations. This is needed when detailed flow in the wellbore and its vicinity is important for accurate predictions. A typical process which requires this approach is the steam-assisted gravity drainage recovery of bitumen described in Stone et al (1989) and Siu et al (1990). Because of the comprehensive treatment of the wellbore, the computing cost of this approach is high and therefore may become prohibitive in large field-scale simulation. Furthermore, in large field-scale simulations, it is not necessary to model the detailed flow phenomena in the horizontal wellbore. A good approximation of the pressure drop and saturation and composition distribution in the wellbore usually suffices.

This paper proposes an efficient technique for field-scale simulation of horizontal wells. The horizontal well is treated as a second porosity in the reservoir. The "porosity" of the wellbore gives the correct wellbore volume. The "permeability" and "relative permeabilities" of the wellbore are adjusted to yield the pressure drop and phase slip from multiphase flow correlations. Because the wellbore flow equations are cast into the same form as the reservoir flow equations, efficient numerical techniques that have been developed for reservoir simulation can be readily used. The dual-porosity representation of horizontal wells is developed for black-oil simulation, and extended for thermal applications as well. In addition, elliptical grid refinement for improved predictions of flow phenomena around the well is developed for black-oil simulation.

Simulation runs with the technique developed are carried out to study the effect of wellbore length and production rate on the oil recovery in a thin reservoir under bottom-water drive, using the black oil model. The elliptical grid refinement is also presented. As an example of the thermal application, a dual horizontal well (injector/producer) steam assisted gravity drainage process is modelled.

2. WELLBORE FLOW EQUATIONS

2.1 Outline

Equations for wellbore flow are presented and transformed into a form similar to Darcy's flow. The equations are first developed for single-phase or homogeneous flow. In the homogeneous flow assumption, the multiphase system behaves like a single-phase system with average properties. Under this assumption, the velocities of all phases are the same (zero slip). The equations are then extended to cases where the phases flow at different velocities (non-zero slip). This isothermal, black oil treatment is generalized to thermal processes in the concluding section.

The modelling of the fluid transfer between wellbore and reservoir is also described.

2.2 Single-Phase and Homogeneous Flow in Wellbore

Figure 1 shows a vertical cross-section of a reservoir with a horizontal well. The well is treated as a second porosity with porosity ϕ_{we} given by

$$\phi_{we} = \frac{\pi r_{we}^2}{\Delta y \cdot \Delta z} \tag{2.1}$$

for a well in the x-direction.

A mechanical energy balance shows that the pressure drop in the wellbore (Govier and Aziz, 1972) is the sum of the pressure drops due to friction, gravity and kinetic energy. Usually, the kinetic energy effect is negligible for wellbore flow conditions. The pressure gradient $\Delta p/\Delta x$ is therefore

$$\frac{\Delta p}{\Delta x} = \underbrace{-\frac{f \bar{\rho} \bar{v}^2}{r_{we}}}_{\text{friction}} + \underbrace{\bar{\rho} g \frac{\Delta z}{\Delta x}}_{\text{gravity}} \tag{2.2}$$

where f is the Fanning friction factor, $\bar{\rho}$ the average mixture mass density, $\bar{v}$ the average mixture velocity, g the gravity acceleration and Δz the change in depth (measure positive downward). When the well is perfectly horizontal, $\Delta z = 0$. For three-phase (oil, gas, water) homogeneous flow

$$\bar{\rho} = \sum_j \rho_j S_j \qquad j=o,g,w \qquad (2.3)$$

where S_j is the saturation of phase j in the wellbore.

The Fanning friction factor f is usually a function of the Reynolds number

$$Re = (d_{we}\ \bar{v}\ \bar{\rho}) / \bar{\mu} \qquad (2.4)$$

with

$$\bar{\mu} = \sum_j \mu_j S_j \qquad (2.5)$$

and the relative roughness of the horizontal well $(e/d)_{we}$. In thermal flow of liquids, the temperature effect on viscosity must also be considered. f increases when the liquid is cooled and decreases when heated.

For laminar flow (Re < 2100), the relative roughness has no effect and

$$f = 16/Re = 8\bar{\mu} / (r_{we}\ \bar{v}\ \bar{\rho}) \qquad (2.6)$$

Substituting Equation (2.6) in Equation (2.2) gives

$$\bar{v} = -\left(\frac{r_{we}^2}{8}\right)\left(\frac{1}{\bar{\mu}}\right)\frac{\Delta\Phi}{\Delta x} \qquad (2.7)$$

where $\Delta\Phi/\Delta x$ is the potential gradient defined as

$$\Delta\Phi/\Delta x = \Delta p/\Delta x - \bar{\rho}\, g\, \Delta z/\Delta x \qquad (2.8)$$

Equation (2.7) is the well known Hagen-Poiseuille equation for laminar flow in a pipe. The fluid velocity with respect to a gridblock cross section is

$$u = \phi_{we}\ \bar{v} = -\phi_{we}\left(\frac{r_{we}^2}{8}\right)\left(\frac{1}{\bar{\mu}}\right)\frac{\Delta\Phi}{\Delta x} \qquad (2.9)$$

Equation (2.9) shows that single-phase or homogeneous laminar flow in the wellbore is similar to the flow in a porous medium (Darcy's law) with effective "permeability"

$$k_{we} = \phi_{we}\, r_{we}^2/8 \tag{2.10}$$

For turbulent flow (Re > 2100), the Fanning friction factor f can be obtained from various correlations available in the literature. Govier and Aziz (1972) recommended the equation due to Colebrook:

$$\frac{1}{\sqrt{f}} = 4 \ln \frac{d_{we}}{2e_{we}} + 3.48 - 4 \ln\left(1 + 9.35 \frac{d_{we}}{2e_{we}\ Re\ \sqrt{f}}\right) \tag{2.11}$$

With $u = \phi_{we}\, \bar{v}$, Equation (2.2) can be rewritten as

$$u = -\phi_{we}\left[\frac{r_{we}}{\bar{\rho} f} \cdot \frac{1}{|\Delta\Phi/\Delta x|}\right]^{\frac{1}{2}} \frac{\Delta\Phi}{\Delta x} \tag{2.12}$$

or

$$u = -\frac{k_{we}}{\bar{\mu}} \frac{\Delta\Phi}{\Delta x} \tag{2.13}$$

with

$$k_{we} = \phi_{we}\, \bar{\mu}\left[\frac{r_{we}}{\bar{\rho} f} \cdot \frac{1}{|\Delta\Phi/\Delta x|}\right]^{\frac{1}{2}} \tag{2.14}$$

Note that the wellbore effective "permeability" in the turbulent flow regime (Equation 2.14) is much more complex than in the laminar flow regime (Equation 2.10). The turbulent-flow permeability depends on the fluid properties, the potential gradient and the friction factor and can be solved for in a fully implicit fashion along with all other variables in the solution of the well equations. In this report, this term is evaluated explicitly, i.e. at the previous time level. Under pseudo-steady-state wellbore flow conditions which occur frequently in field-scale simulation, the pressure gradient and fluid properties do not change drastically between timesteps and therefore explicit evaluation of Equation (2.14) is reasonable.

The individual phase velocities in homogeneous flow are:

$$u_j = - \frac{k_{we}\, k_{rj}}{\bar{\mu}} \frac{\Delta\Phi}{\Delta x} \qquad j=o,g,w \qquad (2.15)$$

with

$$k_{rj} = S_j \qquad (2.16)$$

Equation (2.15) is similar to the multiphase Darcy's law equation except for the use of the mixture average viscosity instead of the phase viscosity. Equation (2.16) corresponds to the use of linear relative permeability curves for the wellbore.

The velocities in Equation (2.15) are Darcy's velocities which are based on the entire gridblock cross section. The actual phase velocities (called in situ velocities) in the wellbore are

$$v_j = u_j / (\phi_{we} S_j) \qquad j=o,g,w \qquad (2.17)$$

Equation (2.17) shows that all phases flow at the same velocity in the wellbore (no slippage nor holdup). Note that u_j is proportional to the superficial velocities v_{sj} commonly used in pipe flow, i.e.

$$v_{sj} = u_j / \phi_{we} \qquad j=o,g,w \qquad (2.18)$$

2.3 Extension to Multiphase Flow With Slippage or Holdup

When phases differ in densities and viscosities, the less dense phase usually flows at a higher in situ velocity. This gives rise to the "slippage" of one phase past the other or "holdup" of one phase relative to the other. Empirical correlations are available to predict slippage/holdup for two-phase gas-liquid horizontal flow in pipes (Govier and Aziz, 1972). These correlations usually express slippage/holdup in terms of the insitu pipe saturation E_g and provide correlation for two-phase friction factors. Since three-phase flow correlations are not available, it is common practice in oil, gas and water systems to lump the oil and water phase into a pseudo single-phase liquid. Experiments with three-phase flows involving light oil, gas and water have shown that they have the same characteristics as gas-liquid two-phase flows. Since slippage between liquid phases is slight, the oil-water

mixture can be represented as a pseudo homogeneous phase. However, this may not be true for heavy oil-water systems and experimental work in this area is required to model the effect.

To model the slippage of the gas phase with respect to the liquid phase, it is proposed to use the gas "relative permeability" k_{rg} in Equation (2.15). k_{ro} and k_{rw} remain equal to S_o and S_w respectively. Each wellbore gridblock can be visualized as a "pipe" and it is desired to match the wellbore gridblock saturation S_g to the in situ gas saturation E_g predicted from a two-phase flow correlation by adjusting k_{rg}. Assume the following form for k_{rg}

$$k_{rg} = \alpha S_g \tag{2.19}$$

Since u_g is linear in S_g from Equation (2.19), a Taylor's series expansion of u_g about S_g=E_g gives

$$u_g(E_g) = u_g(S_g) + (E_g - S_g)\frac{\partial u_g(S_g)}{\partial S_g}$$

$$\approx u_g(S_g) + (E_g - S_g)\frac{u_g(S_g)}{S_g}$$

or

$$u_g(E_g) \approx (E_g/S_g) \cdot u_g(S_g) \tag{2.20}$$

From Equation (2.20), in order for $u_g(S_g)$ to yield $S_g = E_g$, it is necessary to multiply $u_g(S_g)$ by (S_g/E_g). This provides a procedure for finding α in Equation (2.19) as follows:

$$\alpha^{n+1} = \alpha^n \cdot (S_g/E_g)^n \tag{2.21}$$

with

$$\alpha^1 = 1 \tag{2.22}$$

where n denotes the timestep level. The procedure (2.21) gives a time-dependent value of α that tracks the value predicted from the two-phase flow correlation. Under pseudo steady state conditions, the procedure (2.21) will converge to a constant as demonstrated in an example in Section 4.

In this paper, the two-phase flow correlation due to Duckler et al (1964) is used. This correlation is relatively simple to apply and works with reasonable accuracy for most multiphase flow regimes (Anderson and Russell, 1965). It is valid for horizontal, inclined and vertical flow. However, the approach described above is general and can be used with other two-phase flow correlations.

2.4 Wellbore Discretized Equations

The above derivations show how the flow in the wellbore can be transformed into a form similar to Darcy's law. The advantages of using this form and of representing the wellbore as a second porosity are:

i) Numerical techniques that have been developed for reservoir simulation can readily be applied.
ii) The integration in current reservoir-simulation codes is rather simple.
iii) Computer codes that were developed for a dual-porosity naturally-fractured reservoir can be extended to handle wellbore flow.
iv) Wellbore equations are cast in terms of in-situ pressure and saturations instead of velocities. This makes wellbore primary variables consistent with simulator primary variables. This should result in improved convergence of the total system over other coupling techniques.

The fully implicit discretized equations for black oil fluids flowing in the wellbore with the notational convention in reservoir simulation are:

Oil:

$$\Delta T_o^{n+1}\ \Delta\Phi_o^{n+1} + \tau_o^{n+1} + q_o^{n+1} - \frac{V}{\Delta t}\left[(\phi_{we} S_o/B_o)^{n+1} - (\phi_{we} S_o/B_o)^n\right] = 0 \qquad (2.23)$$

Gas:

$$\Delta T_g^{n+1}\ \Delta\Phi_g^{n+1} + \Delta T_o^{n+1}\ R_s^{n+1}\ \Delta\Phi_o^{n+1} + \tau_g^{n+1} + R_s^{n+1}\ \tau_o^{n+1} + q_g^{n+1} - \frac{V}{\Delta t}\left\{[\phi_{we} S_g/B_g + \phi_{we} S_o R_s/B_o]^{n+1} - [\phi_{we} S_g/B_g + \phi_{we} S_o R_s/B_o]^n\right\} = 0 \qquad (2.24)$$

Water:

$$\Delta T_w^{n+1}\ \Delta\Phi_w^{n+1} + \tau_w^{n+1} + q_w^{n+1} - \frac{V}{\Delta t}\left[(\phi_{we}\ S_w/B_w)^{n+1} - (\phi_{we} S_w/B_w)^n\right] = 0 \qquad (2.25)$$

The τ_j's (j=o,g,w) represent the transfer term between the reservoir and wellbore and the q_j's are the source/sink terms corresponding to the injection into the wellbore or production from the wellbore. The above equations are solved simultaneously with the reservoir flow equations. The reservoir equations are discretized using the adaptive-implicit technique (Fung et al, 1989). Following Peaceman's (1983) work on vertical wells in anisotropic reservoirs, the following expression can be derived for τ_j

$$\tau_j = I_{we}\left(\frac{k_{rj}}{\mu_j B_j}\right)(p_{we} - p_j) \qquad j=o,g,w \qquad (2.26)$$

where p_j is the pressure of Phase j in the reservoir gridblock and I_{we} is the well index. I_{we} is calculated from

$$I_{we} = \frac{2\pi\,\bar{k}\,\Delta x}{\ln(r_o/r_w)} \qquad (2.27)$$

$$\bar{k} = (k_y\ k_z)^{\frac{1}{2}} \qquad (2.28)$$

and r_o the equivalent drainage radius obtained from

$$r_o = 0.28\,\frac{\left[(k_z/k_y)^{\frac{1}{2}}\,\Delta y^2 + (k_y/k_z)^{\frac{1}{2}}\,\Delta z^2\right]^{\frac{1}{2}}}{(k_z/k_y)^{\frac{1}{4}} + (k_y/k_z)^{\frac{1}{4}}} \qquad (2.29)$$

2.5 An Alternate Approach: Integration of a Pressure-Drop Equation

An alternate approach for calculating the pressure drop in the horizontal wellbore consists of integrating a pressure drop equation. This is an extension of the method of Aziz et al (1972) for vertical wells to horizontal-well saturations and is also referred to as the simplified-wellbore approach. The horizontal wellbore is discretized into sections conforming to the gridblocks containing them. For each section, a pressure drop equation is

constructed accounting for the frictional and kinetic energy pressure losses as well as the influx (or outflow) of fluids from (or to) the reservoir. The pressure drop differential equation is

$$dp = dp_f + dp_{ke} \tag{2.30}$$

where

$$dp_f = \frac{f \bar{v}^2 \bar{\rho}}{r_{we}} dx \text{ (frictional pressure drop)} \tag{2.31}$$

$$dp_{ke} = \bar{\rho} \bar{v} d\bar{v} \text{ (pressure drop due to kinetic energy effects)} \tag{2.32}$$

Integration of Equations (2.31) and (2.32) gives the pressure drop along the wellbore.

The above approach was found to yield the same pressure drop as in the dual-porosity approach. However, in the pressure-integration method only the pressure drop is calculated. The continuity equations are not solved and therefore the saturation distribution in the wellbore is not known. In contrast, the dual-porosity approach solves these equations and also provides a saturation distribution in the wellbore. Furthermore, the pressure drop in the simplified wellbore approach is not coupled implicitly to the reservoir flow equations, whereas both wellbore pressures and saturations in the dual-porosity approach are solved simultaneously with the reservoir flow equations. This would allow an efficient and rigorous modelling of slip and backflow which is not possible with the pressure-integration approach.

The extension to thermal processes is straightforward with the dual-porosity approach as will be seen later. This is not the case for the integration approach as an additional ordinary differential equation for the temperature is required. This temperature equation is strongly coupled to the pressure equation which makes the whole system more difficult to solve.

For the above reasons, the dual-porosity approach for modelling wellbore flow is preferred over the integration approach.

2.6 Extension of Dual-Porosity Approach to Thermal Simulation

The dual-porosity concepts and implementation can be extended to a thermal simulation in a relatively straightforward manner. Because a thermal simulator solves a set of component flow equations coupled with an equation for energy flow, the only essentially new element is a consideration of the latter. The component flow equations remain

equivalent to those given by Equations (2.23), (2.24) and (2.25) - for a two component oil - except that the water component flow equation contains additional terms accounting for the possible presence of steam. The phase transfer terms τ_j (j=o,g,w) between reservoir and wellbore remain unchanged. For brevity, the form of these equations in our thermal simulator are not repeated here.

The energy flow equation can be written as

$$\sum_j \Delta T_j^{n+1} H_j^{n+1} \Delta\Phi_j^{n+1} + \Delta T_c^{n+1} \Delta\theta^{n+1} + \sum_j H_j^{n+1} \tau_j + \tau_c + q_U^{n+1} + h_j^{n+1}$$

$$- \frac{V}{\Delta t} \left\{ \sum_j (\phi_{we} S_j U_j/B_j)^{n+1} - \sum_j (\phi_{we} S_j U_j/B_j)^n \right\} \qquad (2.33)$$

Here, the convective heat transfer between wellbore and reservoir is seen to involve the phase enthalpies H_j (j=o,g,w) and the same transfer terms τ_j that appear in the component flow equations. In addition, conductive heat transfer between the wellbore and the reservoir arises

$$\tau_c = 2\pi \Delta x \kappa \frac{\theta_{we} - \theta}{\ln (r_\theta/r_{we})} \qquad (2.34)$$

involving the temperature difference between wellbore, θ_{we}, and reservoir, θ, the appropriate block thermal conductivity κ (either wellbore or reservoir values are used depending on temperature upstream), and a geometric factor which includes r_θ, the equivalent thermal drainage radius

$$r_\theta = 0.14 \sqrt{(\Delta y^2 + \Delta z^2)} \qquad (2.32)$$

This latter expression is the isotropic equivalent of (2.29).

The flow of heat in the wellbore and the transfer of energy between the wellbore and the reservoir, in part, determines the local values of phase saturations and phase velocities occurring in the wellbore. These values are then used in the wellbore flow correlations presented in Sections 2.2 and 2.3.

3. HYBRID GRID

3.1 Outline

The treatment of flow in the vicinity of the wellbore can have a large impact on the simulation results. Cartesian grid systems are commonly used to represent the reservoir. The sizes of these gridblocks are much larger than the diameter of the well (usually two to three orders of magnitude). Equations (2.27)-(2.29) derived by Peaceman (1983) give the well index I_{we} which relates flow rates to the gridblock pressure and well pressure. The mobilities used in calculating the rates in Equation (2.26) correspond to the coarse Cartesian gridblock saturation. Because of the converging (diverging) flow phenomena around a producer (injector), steep saturation gradients occur in the vicinity of the well. Therefore, the coarse Cartesian grid may not provide enough resolution for accurate calculations of well inflow (or outflow) and leads to errors in the predictions of water cut, gas-oil ratio and breakthrough times.

To obtain good resolution in the vicinity of the wellbore, a fine grid spacing around the wellbore is often used. Early grid refinement techniques used Cartesian grids (Heinemann et al, 1983; Forsyth and Sammon, 1985; Quandalle and Besset, 1985; Wasserman, 1987). More recent publications by Pedrosa and Aziz, 1986 and Ewing et al, 1989 show that for vertical wells in a reservoir with isotropic permeabilities in the areal directions, the use of circular cylindrical grid refinement within a Cartesian grid provides an efficient and accurate approach for modelling near-well phenomena. The Cartesian coarse grids with the cylindrical refined grids are called hybrid grids.

In this section, a hybrid grid system is developed to model flow phenomena near a horizontal well. Because the vertical permeability and horizontal permeability are usually different, elliptical cylindrical grids are required. The following development is a generalization of Pedrosa's approach (Pedrosa, 1984) for vertical wells in anisotropic media to horizontal wells.

3.2 Elliptical Grid Refinement

Figure 2 shows a vertical section of a reservoir containing a horizontal well. The permeability k_y in the horizontal direction is greater than the permeability k_z in the vertical direction. Consider the transformation

$$y' = y\,(\bar{k}/k_y)^{\frac{1}{2}} \tag{3.1}$$

$$z' = z\,(\bar{k}/k_z)^{\frac{1}{2}} \tag{3.2}$$

where

$$\bar{k} = (k_y \cdot k_z)^{\frac{1}{2}} \tag{3.3}$$

In the transformed coordinate system, the well is an ellipse with semi-focal length

$$L_{we} = r_{we}\left[(k_y - k_z)/\bar{k}\right]^{\frac{1}{2}} \tag{3.4}$$

semi-major axis

$$a_{we} = r_{we}\,(\bar{k}/k_z)^{\frac{1}{2}} \tag{3.5}$$

and semi-minor axis

$$b_{we} = r_{we}\,(\bar{k}/k_y)^{\frac{1}{2}} \tag{3.6}$$

Under incompressible, single-phase, steady-state flow, equipotential lines are confocal ellipses of semi focal length L_{we} in the transformed coordinate system (y', z') as in the case for vertical wells. This is true since, under these assumptions T is constant and hence $\Delta T \Delta \Phi$ becomes $T\Delta(\Delta\Phi)$. But $\Delta\Phi = \Delta p - \rho g \Delta z$ and since we are assuming incompressibility, $\Delta\rho$ and hence $\Delta\rho g \Delta z$ are both zero. The stream lines are hyperbolas orthogonal to those ellipses. This is the natural coordinate system for the flow around the wellbore. Figure 3 shows the local grid refinement in the elliptical coordinate system.

The elliptical coordinate system may be defined by the equations

$$z' = L_{we} \cosh \xi \cos \eta \tag{3.7}$$

$$y' = L_{we} \sinh \xi \sin \eta \tag{3.8}$$

with $\xi \geq 0$ and $0 \leq \eta < 2\pi$. A curve ξ = constant is an ellipse with semi axes $L_{we} \cosh \xi$ in the z' direction and $L_{we} \sinh \xi$ in the y' direction. A curve η = constant is half of one branch

of an hyperbola with semi-axes $L_{we}\cosh\xi$ and $L_{we}\sinh\xi$.

If the coarse Cartesian grid system is chosen so that the transformed Cartesian grid is square, and if the well dimensions are much smaller than the coarse-grid dimension (which is usually the case), the hyperbolas associated with the gridblock boundaries correspond to $\eta = \frac{k\pi}{4}$, k=1,2,3,4. The η's for the gridnodes are therefore $\eta = \frac{k\pi}{2}$, k=0,1,2,3.

The ellipses associated with the gridblock boundaries in the ξ direction are determined as follows. Let ξ_{we} be the ellipse corresponding to the well. The next ellipse is defined by $\xi_{1+\frac{1}{2}}$ such that the area of that ellipse is $\Delta y' \cdot \Delta z'/(n_r+1)^2$ where n_r is the number of radial direction subdivisions around the well. The area within an ellipse is

$$A = \frac{\pi}{2} L_{we}^2 \sinh 2\xi \tag{3.9}$$

The outer ellipse $\xi_{n_r+\frac{1}{2}}$ is defined such that the area is equal to $\Delta y' \cdot \Delta z'$. The boundaries of the intermediate ellipses are at every

$$\Delta\xi = \frac{\xi_{n_r+\frac{1}{2}} - \xi_{1+\frac{1}{2}}}{n_r - 1}$$

The above selection of grid boundaries follows our experience on designing radial grid refinement for vertical wells in isotropic media. The location of the gridnodes within these ellipses follows the recommendation of Pedrosa (1984) who derived it from a steady-state flow analysis

$$\xi_i = \frac{\left(\xi_{i+\frac{1}{2}} \sinh 2\xi_{i+\frac{1}{2}} - \xi_{i-\frac{1}{2}} \sinh 2\xi_{i-\frac{1}{2}}\right) - 0.5\left(\cosh 2\xi_{i+\frac{1}{2}} - \cosh 2\xi_{i-\frac{1}{2}}\right)}{\sinh 2\xi_{i+\frac{1}{2}} - \sinh 2\xi_{i-\frac{1}{2}}} \tag{3.10}$$

The discretized oil phase equation in the elliptical refined grid is:

$$\Delta T_{\xi_o} \Delta\Phi_o + \Delta T_{\eta_o} \Delta\Phi_o + q_o - \frac{V}{\Delta t}\left[\left(\frac{\phi S_o}{B_o}\right)^{n+1} - \left(\frac{\phi S_o}{B_o}\right)^{n}\right] = 0 \tag{3.11}$$

where

$$T_{\xi_o} = \frac{\bar{k}\,\Delta x\,\Delta\eta}{\Delta\xi}\,\frac{k_{ro}}{\mu_o B_o} \tag{3.12}$$

$$T_{\eta_o} = \frac{\bar{k}\,\Delta x\,\Delta\xi}{\Delta\eta}\,\frac{k_{ro}}{\mu_o B_o} \tag{3.13}$$

$$\Delta\Phi_o = \Delta p - \gamma_o\,\Delta D \tag{3.14}$$

Similar equations can be written for the gas and water.

An example in Section 4 will illustrate the use of elliptical grid refinement around a horizontal well.

4. EXAMPLES

4.1 Outline

In Section 4.2, the techniques developed are used to predict the performance of horizontal wells in a black-oil reservoir which is under bottom water drive. Both gas cusping and water coning are important. The effect of rates and lengths on the recovery is examined.

In Section 4.3, elliptical grid refinement is applied to one of the cases in Section 4.2. The results obtained are discussed.

In Section 4.4, the dual-porosity representation of the well is applied to a steam-assisted gravity drainage process.

4.2 Light Oil Recovery From a Horizontal Well

The technique developed is used to predict the performance of horizontal wells in a reservoir which is under bottom water drive. Both gas cusping and water coning are important. The effect of rates and lengths on the recovery is examined.

Table 1 shows a cross-section of a reservoir where the thin oil producing layers are sandwiched between a gas cap and a bottom water layer. The horizontal permeabilities (k_x and k_y) are 300 md and the vertical permeability is 30 md. The reference porosity ϕ^* is 0.20. Also shown in Table 1 are the initial conditions of the reservoir.

Fluid property data are from the Fifth SPE Comparative Solution Project (Killough and Kossak, 1987). However, the reservoir, relative permeabilities and capillary pressures are different from those in the above reference. Fluid property data are given in Table 2 and relative-permeability and capillary-pressure data are reported in Table 3. The initial bubble-point pressure is equal to the gridblock oil pressure in each gridblock.

The reservoir is represented by a 9x9x8 grid system. The gridblock dimensions in the horizontal directions (x and y directions) are shown in Figure 4. The thicknesses in the vertical direction (z direction) are reported in Table 1.

Fluids are produced from a horizontal well drilled in Layer 4. The well passes through the gridblock centers and the entire length is open to flow. Two lengths are considered:

a) L = 900 ft (274 m), well completed in Gridblocks (I,5,4), I=6,7,8
b) L = 2100 ft (640 m), well completed in Gridblocks (I,5,4), I=2,3,...8

Fluids are removed from the portion of the well in Gridblock (8,5,4) to the surface. The horizontal wellbore has an inside diameter of 4.5 inches (0.1143 m) and an effective relative roughness of 10^{-3}.

A constant pressure line source is used to simulate the bottom water drive. The line source is completed in Gridblocks (I,5,6), I=1,2,...,9 and is maintained at a constant pressure of 3080 psia (21236 kPa).

The horizontal well produces at a constant liquid (oil and water) rate. Two rates Q_l are considered: 3000 STB/day (477 std m^3/day) and 6000 STB/day (954 std m^3/day). Each production rate is examined for two well lengths, giving four cases altogether

Case 1: L = 900 ft (274 m)
Q_l = 3000 STB/day (477 std m^3/day)

Case 2: L = 2100 ft (640 m)
Q_l = 3000 STB/day (477 std m^3/day)

Case 3: L = 900 ft (274 m)
Q_l = 6000 STB/day (954 std m^3/day)

Case 4: L = 2100 ft (640 m)
Q_l = 6000 STB/day (954 std m^3/day)

Figures 5 through 13 show the predictions obtained for the four cases. The following observations can be made:

1. Increasing the well length improves the oil recovery: less water coning and gas cusping which yield later water and gas breakthrough (Figures 5 and 6), increased oil

recovery (Figures 7 and 8), less water produced (Figures 9 and 10), and less gas produced (Figures 11 and 12).

2. The production rates influence the coning and cusping behavior. Less coning and cusping are observed with the lower rate as expected. Figure 5 shows that in Case 2 no cusping of gas was detected.

3. As large amounts of water cone up into the gridblocks containing the wellbore, they interfere with the gas flow and reduce the GOR. This can clearly be seen in Figure 6 for Case 3.

4. Typical changes of S_g and E_g and of α in Equation (2.21) versus time are shown in Figure 13. Values are reported for the well block in Gridblock (8,5,4) for Case 3. During the early stage of production ($t < 100$ days), α exhibits an erratic behavior because of the small gas saturation in the wellbore (<5%). As the gas saturation builds up in the wellbore, a gradual change of α is observed. The results show that S_g tracks E_g predicted by Dukler et al correlation very adequately. S_g and E_g cannot be identical because of the explicit update in Equation (2.21), but the differences are small. Figure 13 also shows that, as pseudo-steady-state conditions prevail at larger time, α tends toward a constant value. This approach is therefore very attractive because it reduces considerably the computational effort that would have been required if a fully implicit solution of the two-phase flow correlation was adopted.

5. The pressure drops along the two well lengths of 900 ft (274 m) and 2100 ft (640 m) for a liquid rate of 3000 STB/day (477 std m^3/day) are 0.47 psia (3.2 kPa) and 0.82 psia (5.7 kPa) respectively. For a total liquid rate of 6000 STB/day (954 std m^3/day) the calculated pressure drop is 1.53 psia (10.6 kPa) for L=900 ft (274 m) and 3.44 psia (23.7 kPa) for L = 2100 ft (640 m).

4.3 Elliptical Grid Refinement

Elliptical grid refinement was applied to the coarse grid containing the horizontal well in Case 3. Three ellipses were used in the ξ direction and four subdivisions in the η direction were used.

Figure 14 compares the water cuts and gas oil ratios of Case 3 with and without elliptical grid refinement. This figure shows that the water-cut predictions are similar but differences exist in the gas-oil ratio predictions.

To validate the hybrid-grid options, additional runs were performed with two and four ellipses around the well with four subdivisions in the η direction. The predicted gas-oil ratios are shown in Figure 15. The plots show that as the grid is refined, the results converge to a same curve. This demonstrates the validity of the hybrid-grid refinement technique.

4.4 Steam Assisted Gravity Drainage

As a thermal example of the techniques developed in this project, a dual horizontal well (injector and producer) steam assisted gravity drainage scenario is simulated, based on a modified Lee and Tan (1987) configuration. A symmetry element (one quarter of a reservoir containing overlying horizontal wells) was chosen, with dimensions of 600 ft x 100 ft x 50 ft, and with one-half well lengths of 400 ft. Fifteen years of production were simulated, with both injector and producer being constant-pressure wells. Further simulation data are given in Table 4 and by Lee and Tan (1987). (In addition to ignoring the naturally fractured nature of the Lee and Tan reservoir, we have adjusted the oil viscosity upwards to that of bitumen).

Figures 16 and 17 compare simulated oil production response (cumulative and instantaneous, respectively) of the new wellbore model with the simple, traditional source/sink model. The basic reservoir response is similar, but a significant shift in the onset of oil production occurs (550 days (new model) versus 1000 days (traditional model)).

As viewed from a vertical (y-z) cross section perpendicular to the well directions (Figure 18), the four peaks in instantaneous oil production (Figure 17) correspond roughly to the upward growth of the steam chamber in the first column of gridblocks (directly above the wells), followed by downward growth in the succeeding 3 gridblock columns transverse to the wells (y direction is discretized into 4 columns - see Figure 18). The latter oil production peaks broaden as the steam chamber moves outward via a tangential growth mechanism. Except for the shift in time of initial production, this behavior is reproducible in the two runs. No steam appeared in the (large) gridblocks beyond the wells (areal view I=5 gridblocks).

Several sensitivity runs were conducted to ascertain the origin of the discrepancy. The effects of the wellbore flow correlation (slippage, homogeneous flow, laminar flow) were found to be negligible since the Reynolds number rarely exceeded values greater than 1000. A low Reynolds number early in the run was attributed to low injection/production rates. Once thermal communication was established, higher flow rates ocurred. However, the Reynolds number remained relatively low because of the reduced oil viscosity at the higher temperatures. The role of the conductive heat transfer (setting $\tau_c \equiv 0$) was also found to be minimal (5 day shift in onset time).

The dominant factor in this example appears to be related to the (thermal) wellbore injectivity estimates utilized in the two models. The source well model employs reservoir mobility values (downstream of the wellbore) to calculate injectivity, while the new well model follows standard dual porosity ideas based on upstream (wellbore) mobility estimates for injectivity. By employing the source well model for the injector, the new well model approach for the producer gives the same onset time as simulations utilizing the traditional sink production model.

Further study is required to establish how universal are the conclusions from this simulated example. In particular, in a gravity drainage process, it would be useful to see the impact of increased well length and increased pressure difference between injector and producer (increased flow rates) on the observed wellbore flow regime. Steam cycling and steam drive processes with horizontal wells should also be examined with these ideas in mind.

5. CONCLUSIONS

This paper describes a technique for modelling efficiently horizontal wells in field-scale simulation. The novelty of the technique stems from the casting of the wellbore flow equations into a form similar to the reservoir flow equations. This approach allows the use of efficient numerical techniques that have been developed for reservoir simulation to solve simultaneously for both the reservoir and wellbore variables.

The technique has been implemented first in a black-oil simulator. Test runs in a thin reservoir subjected to bottom water drive show the effect of wellbore lengths and production rates on the recovery. This technique will provide a very valuable tool in the design of well lengths, locations and optimal flow rates. The use of elliptical grid refinement around the wellbore is also presented. This technique allows a more accurate modelling of flow phenomena in the vicinity of the wellbore.

While the implementation and extension of this dual-porosity approach for modelling horizontal wells to thermal simulation proved relatively straightforward, results from a simulated gravity drainage process indicated that different flow mechanisms dominated. In particular, lower flow rates, temperature effects on oil viscosity, and thermal transient effects all appeared to contribute to an increased emphasis on early time, laminar flow behavior in this example. Further study is required to establish how universal are the conclusions from this example. In particular, in a gravity drainage process, it would be useful to see the impact of increased well length and increased pressure difference between injector and producer (increased flow rates) on the observed wellbore flow regime. Steam cycling and steam drive processes with horizontal wells should also be examined with these ideas in mind.

6. NOMENCLATURE

a_{we}	semi-major axis
A	area
b_{we}	semi-minor axis
B_j	formation volume factor j=o,w,g
d_{we}	wellbore diameter
dp	pressure drop differential
e_{we}	wellbore roughness
E	correlation in situ volume fraction
f	Fanning friction factor
g	acceleration due to gravity
h	heat loss to overburden, underburden
H_j	phase enthalpies j=o,w,g
I_{we}	well index
k	absolute permeability
k_r	relative permeability
k_{we}	effective wellbore permeability
L	well length
L_{we}	semi-focal length
n_r	number of radial subdivisions
p	pressure
p_c	capillary pressure
p_{we}	well bottom hole pressure
q	volumetric flow rate
Q	well production rate
r_o	equivalent drainage radius
r_θ	equivalent thermal drainage radius
r_{we}	wellbore radius
Re	Reynolds number
R_s	solution gas ratio
S	saturation
t	time
T	transmissibility
u	saturation averaged Darcy fluid velocity
u_j	Darcy phase velocity j=o,w,g

U_j	internal energy of phase j=o,w,g
$\bar{v}$	average mixture velocity
v_j	phase velocities j=o,w,g
v_s	superficial velocity
V	gridblock volume
α	parameter defined in Equation (2.21)
γ	specific weight
Δp	pressure difference
Δt	timestep size
Δx	gridblock dimension in x-coordinate
Δy	gridblock dimension in y-coordinate
Δz	gridblock dimension in z-coordinate
$\Delta\Phi$	potential difference
η	hyperbolic coordinate
θ,θ_{we}	temperature of gridblock and wellbore, respectively
κ	thermal conductivity
μ_j	phase viscosity j=o,w,g
$\bar{\mu}$	average mixture viscosity
ξ	elliptical coordinate
ρ_j	phase density j=o,w,g
$\bar{\rho}$	average mixture density
τ_j	transfer term between reservoir and wellbore j=o,w,g and c
ϕ_{we}	effective wellbore porosity
ϕ^*	reference porosity
Φ	potential

Subscripts

c	conductive heat
f	friction
g	gas phase
ke	kinetic energy
o	oil phase
s	superficial
U	internal energy
w	water phase

we	wellbore
x	x-coordinate direction
y	y-coordinate direction
z	z-coordinate direction

Superscripts

n	time level
-	average
′	transformed

7. ACKNOWLEDGEMENTS

This research was supported by the Members of the Computer Modelling Group and by the Canada Centre for Mineral Energy Technology (CANMET).

8. REFERENCES

Anderson, R.J., and Russell, T.W., "Designing for Two-Phase Flow - Part II," Chem. Eng., Dec. 20, 1965, pp. 99-104.

Aziz, K., Govier, G.W., and Fogarasi, M., "Pressure Drop in Wells Producing Oil and Gas," J. Can. Pet. Tech., July-Sept. 1972, pp. 38-48.

Butler, R.M., "The Potential of Horizontal Wells for Petroleum Production," Paper 88-39-22, presented at the 39th Annual Technical Meeting of the Petroleum Section of CIM, Calgary, June 1988, pp. 51-56.

Duckler, A.E., Wicks, M., and Cleveland, R.G., "Frictional Pressure Drop in Two-Phase Flow: An Approach Through Similarity Analysis," A.I.Ch.E. J., Vol. 10, Jan. 1964, pp. 44-51.

Ewing, R.E., Boyett, B.A., and Babu, D.K., "Efficient Use of Locally Refined Grids for Multiphase Reservoir Simulation," Tenth SPE Symposium on Reservoir Simulation, Houston, (SPE paper 18413), February 1989, pp. 55-70.

Forsyth, P.A., and Sammon, P.H., "Local Mesh Refinement and Modelling of Faults and Pinchouts," Eighth SPE Symposium on Reservoir Simulation, Dallas, (SPE paper 13524), February 1985, pp. 267-278.

Fung, L.S.K., Collins, D.A., and Nghiem, L.X., "An Adaptive-Implicit Switching Criterion Based on Numerical Stability Analysis," SPE Reservoir Engineering, Feb. 1989, pp. 45-51.

Heinemann, Z.E., Montanuniversität, L., Günter, G., von Hantelmann, G., and Preussag, A.G., "Using Local Grid Refinement in a Multiple-Application Reservoir Simulator," Seventh SPE Symposium on Reservoir Simulation, San Francisco, (SPE paper 12255), November 1983, pp. 205-218.

Karisson, H., and Bitto, R., "Worldwide Experience Shows Horizontal Well Success," World Oil, 1989, pp. 51-56.

Killough, J.E., and Kossack, C.A., "Fifth Comparative Solution Project: Evaluation of Miscible Flood Simulators," SPE Paper 16000, 1987, pp. 55-73.

Lee, B.Y.Q., and Tan, T.B.S., "Application of a Multiple Porosity/Permeability Simulator in Fractured Reservoir Simulation," Ninth SPE Symposium on Reservoir Simulation, (SPE paper 16009), February 1987, pp. 181-192.

Peaceman, D.W., "Interpretation of Well-Block Pressures in Numerical Reservoir Simulation with Nonsquare Grid Blocks and Anisotropic Permeability," Soc. Pet. Eng. J., Vol. 23, No. 3, June 1983, pp. 531-543.

Pedrosa, O.A., and Aziz, K., "Use of Hybrid Grid in Reservoir Simulation," Eighth SPE Symposium on Reservoir Simulation, Dallas, (SPE paper 13507), February 1985, pp. 99-112.

Pedrosa, O.A., "Use of Hybrid Grid in Reservoir Simulation, 1984, Ph.D. Thesis, Stanford University.

Quandelle, P., and Besset, P., "Reduction of Grid Effects Due to Local Sub-Gridding in Simulations Using a Composite Grid," Eighth SPE Symposium on Reservoir Simulation, Dallas, (SPE paper 13527), February 1985, pp. 295-306.

Siu, A., Li, Y.-K., Nghiem, L., and Redford, D.A., "Numerical Modelling of a Thermal Horizontal Well," Paper CIM/SPE 90-122, presented at the CIM/SPE International Technical Meeting, June 10-13, 1990, Calgary, Alberta.

Stone, T.W., Edmunds, N.R., and Kristoff, B.J., "A Comprehensive Wellbore/Reservoir Simulator," Paper SPE 18419, presented at the 10th SPE Symposium on Reservoir Simulation, Houston, February 6-8, 1989.

Wasserman, M.L., "Local Grid Refinement for Three-Dimensional Simulators," Ninth SPE Symposium on Reservoir Simulation, February 1987, pp. 231-242.

Table 1: Reservoir Cross Section and Initial Conditions

Layer	Thickness ft (m)	p_o psia (kPa)	S_o	S_g	S_w
1	30 (9.14)	3000 (20684)	0.319	0.461	0.220
2	20 (6.10)	3006 (20726)	0.780	0.000	0.220
3	20 (6.10)	3011 (20760)	0.780	0.000	0.220
4	20 (6.10)	3016 (20795)	0.780	0.000	0.220
5	20 (6.10)	3020 (20822)	0.780	0.000	0.220
6	20 (6.10)	3025 (20857)	0.780	0.000	0.220
7	30 (9.14)	3031 (20898)	0.594	0.000	0.406
8	50 (15.24)	3046 (21001)	0.000	0.000	1.000

Table 2: Fluid Property Data

Saturated Properties					
Pressure	Solution GOR	Oil FVF	Gas Expansion Factor	Oil Viscosity	Gas Viscosity
(psia)	R_s (SCF/STB)	B_o (RB/STB)	E_g (MSCF/RB)	μ_o (cp)	μ_g (cp)
14.7	0	1.0348	.00473	.310	.0107
500	117.6	1.1017	.1688	.295	.0127
1000	222.6	1.1478	.3508	.274	.0134
1200	267.7	1.1677	.4266	.264	.0138
1500	341.4	1.1997	.5418	.249	.0145
1800	421.5	1.2350	.6578	.234	.0153
2000	479.0	1.2600	.7352	.224	.0159
2302.3	572.8	1.301	.8510	.208	.0170
2500	572.8	1.2958	.9070	.214	.0170
3000	572.8	1.2839	1.015	.227	.0170
3500	572.8	1.2734	1.097	.240	.0170
4000	572.8	1.2639	1.160	.253	.0170
4500	572.8	1.2554	1.216	.265	.0170
4800	572.8	1.2506	1.245	.272	.0170

Oil compressibility for undersaturated oil ($psia^{-1}$)	2.185×10^{-5}
Oil viscosity compressibility for undersaturated oil ($psia^{-1}$)	2.185×10^{-5}
Stock tank oil density, ρ_{ost} (lb_m/ft^3)	38.53
Standard-condition gas density, ρ_{gsc} (lb_m/ft^3)	0.06864
Water compressibility, c_w ($psia^{-1}$)	3.3×10^{-6}
Water formation volume factor at reservoir temperature and atmospheric pressure, B_w^*(RB/STB)	1.0
Water density at standard conditions, ρ_w^* (lb_m/ft^3)	62.4
Reference pressure for water FVF and densities, p_w^*(psia)	14.7
Water viscosity, μ_w (cp)	0.70
Porosity	

Table 3: Relative Permeabilities and Capillary Pressures

Water/Oil Functions

S_w	k_{rw}	k_{row}	P_{cow} (psia)
0.22	0.00	1.0000	7.0
0.30	0.07	0.4000	4.0
0.40	0.15	0.1250	3.0
0.50	0.24	0.0649	2.5
0.60	0.33	0.0048	2.0
0.80	0.65	0.0000	1.0
0.90	0.83	0.0000	0.5
1.00	1.00	0.0000	0.0

Gas/Oil Functions

S_g	k_{rg}	k_{rog}	P_{cgo} (psia)
0.00	0.0000	1.00	0.0
0.04	0.0000	0.60	0.2
0.10	0.0220	0.33	0.5
0.20	0.1000	0.10	1.0
0.30	0.2400	0.02	1.5
0.40	0.3400	0.00	2.0
0.50	0.4200	0.00	2.5
0.60	0.5000	0.00	3.0
0.70	0.8125	0.00	3.5
0.78	1.0000	0.00	3.9

Table 4: Selected Simulation Parameters
Steam Assisted Gravity Drainage Process

Reservoir:	600 ft x 100 ft x 50 ft (5 x 4 x 10 grid)
Gridblocks:	I = 40 ft, 80 ft, 120 ft, 160 ft, 200 ft J = 10 ft, 20 ft, 30 ft, 40 ft K = 5 ft (10 blocks)
Permeability/porosity:	k_x = 2000 md k_y = 2000 md k_z = 2000 md ϕ = 0.30
Oil viscosity:	at initial reservoir temperature (125°F); μ = 7839 cp at steam temperature (358°F); μ = 12.0 cp
Remaining parameters:	see Lee and Tan (1987)
Horizontal injector:	location I=1, 2, 3, 4; J=1; K=2 constant pressure = 155 psia
Horizontal producer	location I=1, 2, 3, 4; J=1; K=1 constant pressure = 154 psia
Simulation time:	15 years

Figure 1: Reservoir Cross Sections with a Horizontal Well

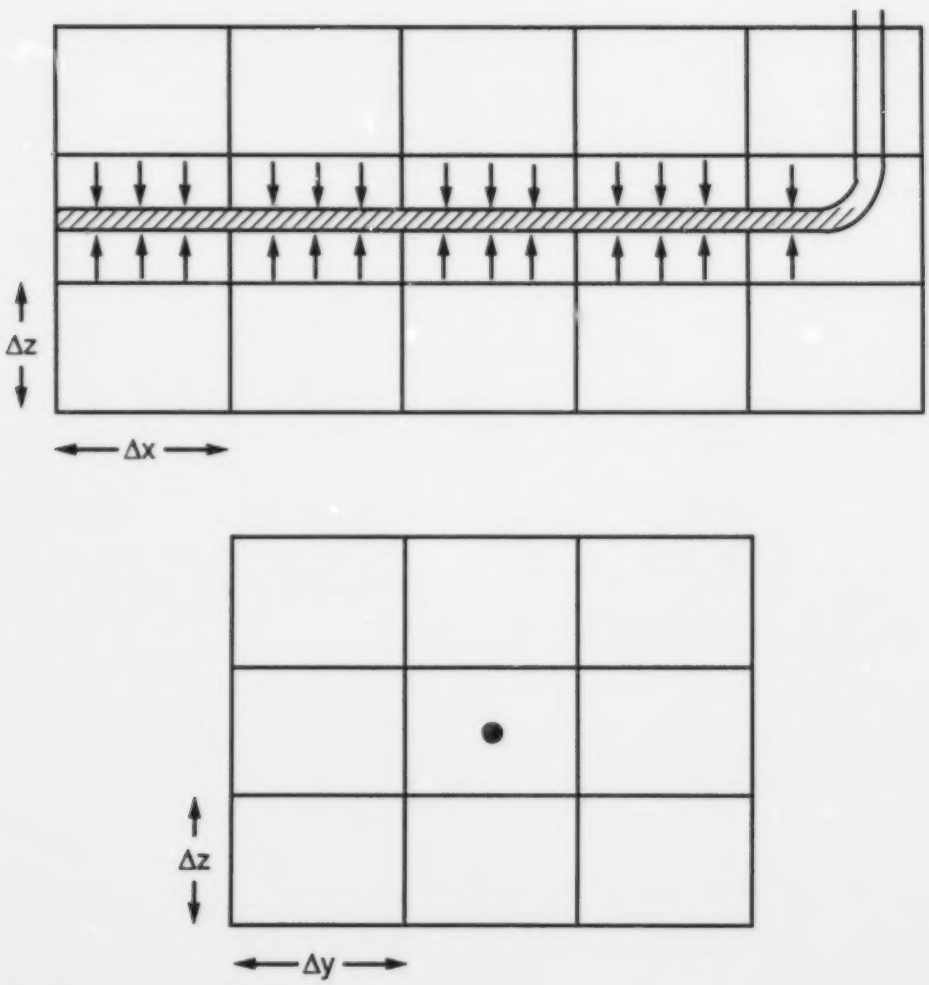

Figure 2: Transformation of a Homogeneous, Anisotropic with a Circular Well to an Equivalent Homogeneous, Isotropic Reservoir

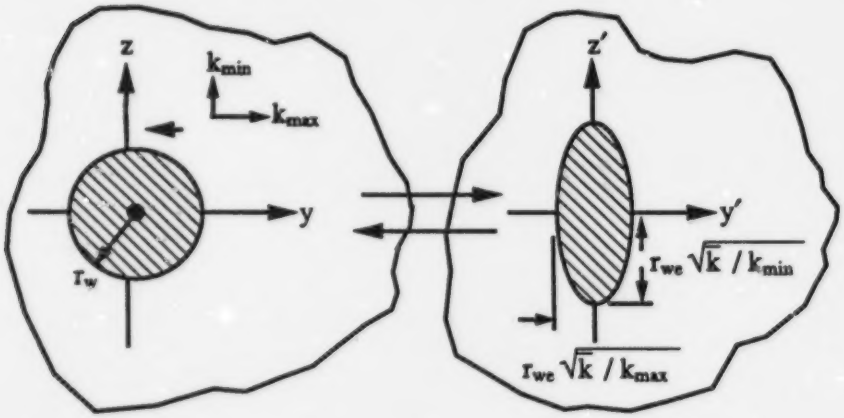

ACTUAL RESERVOIR TRANSFORMED RESERVOIR

Figure 3: Elliptical Grid Refinement Around the Horizontal Well

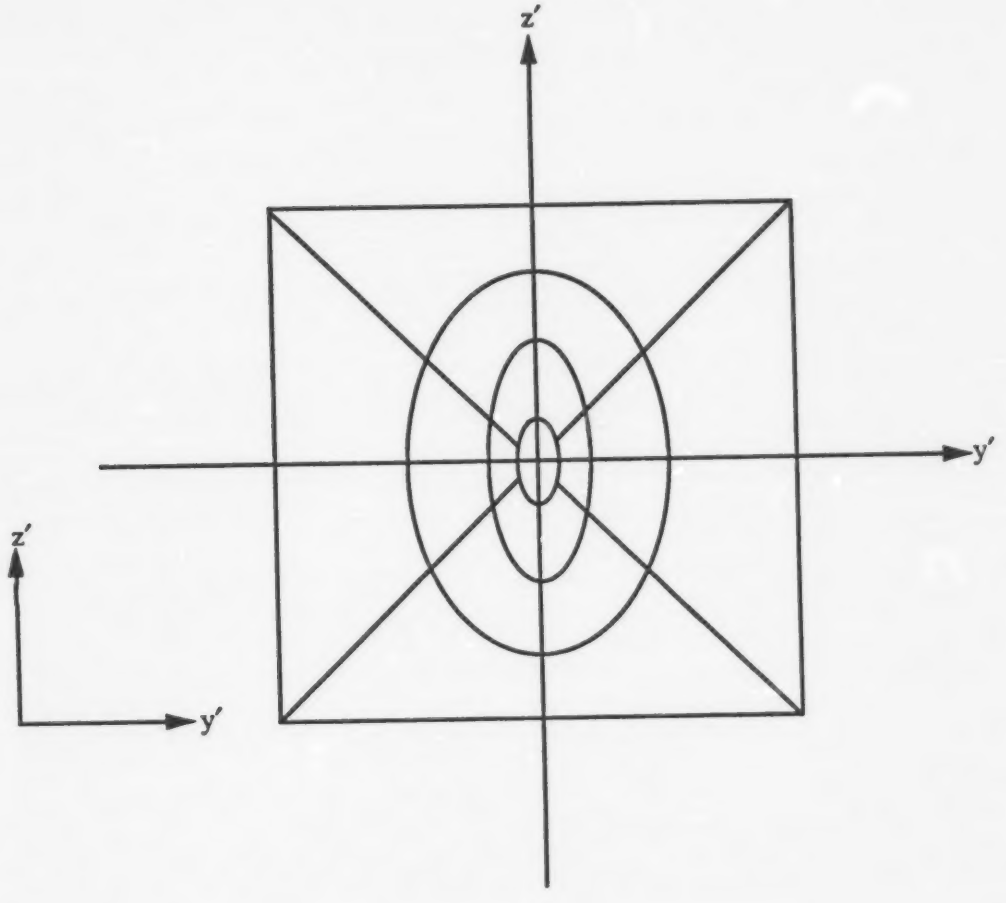

Figure 4: Horizontal Producer in Layer 4

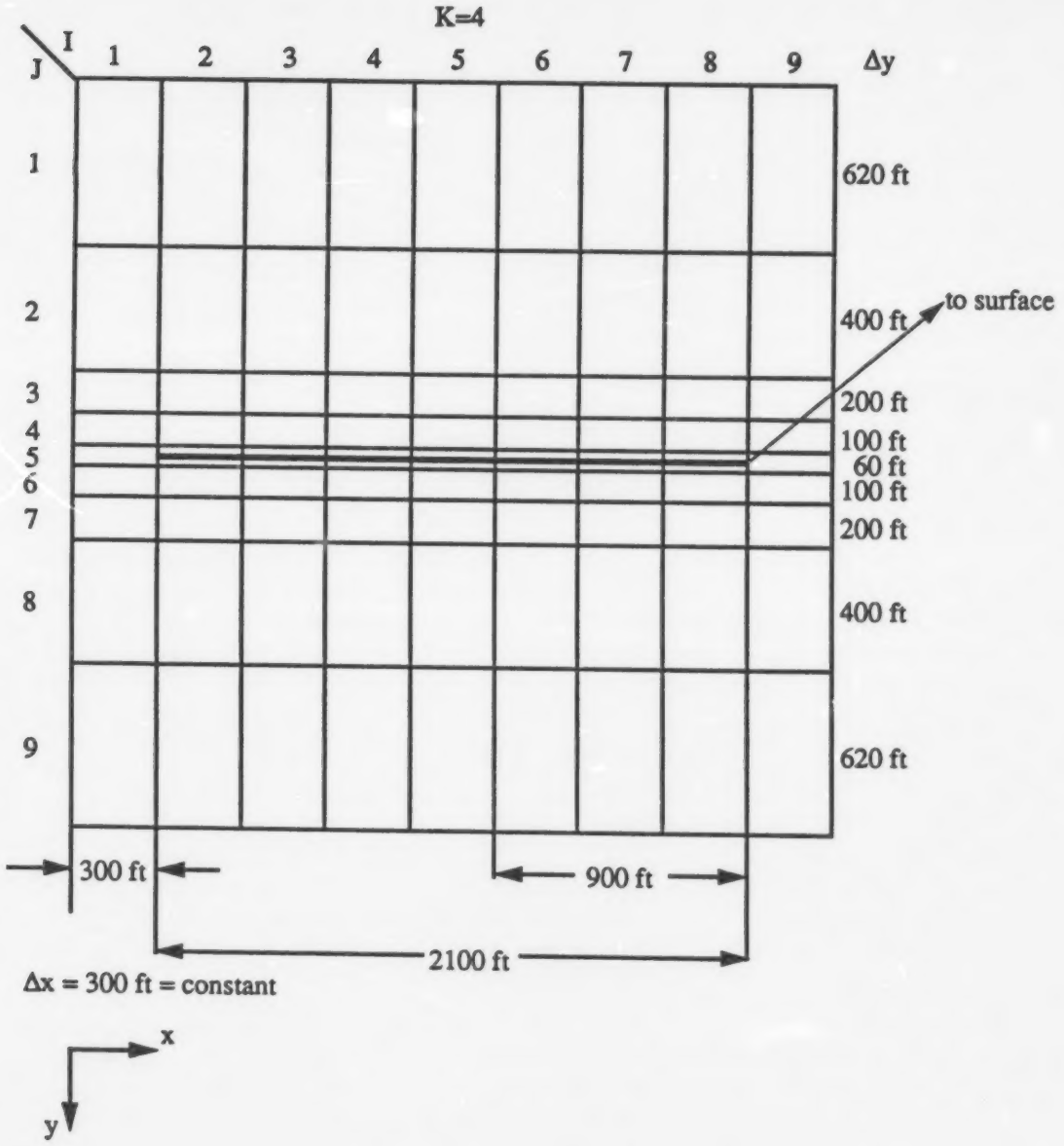

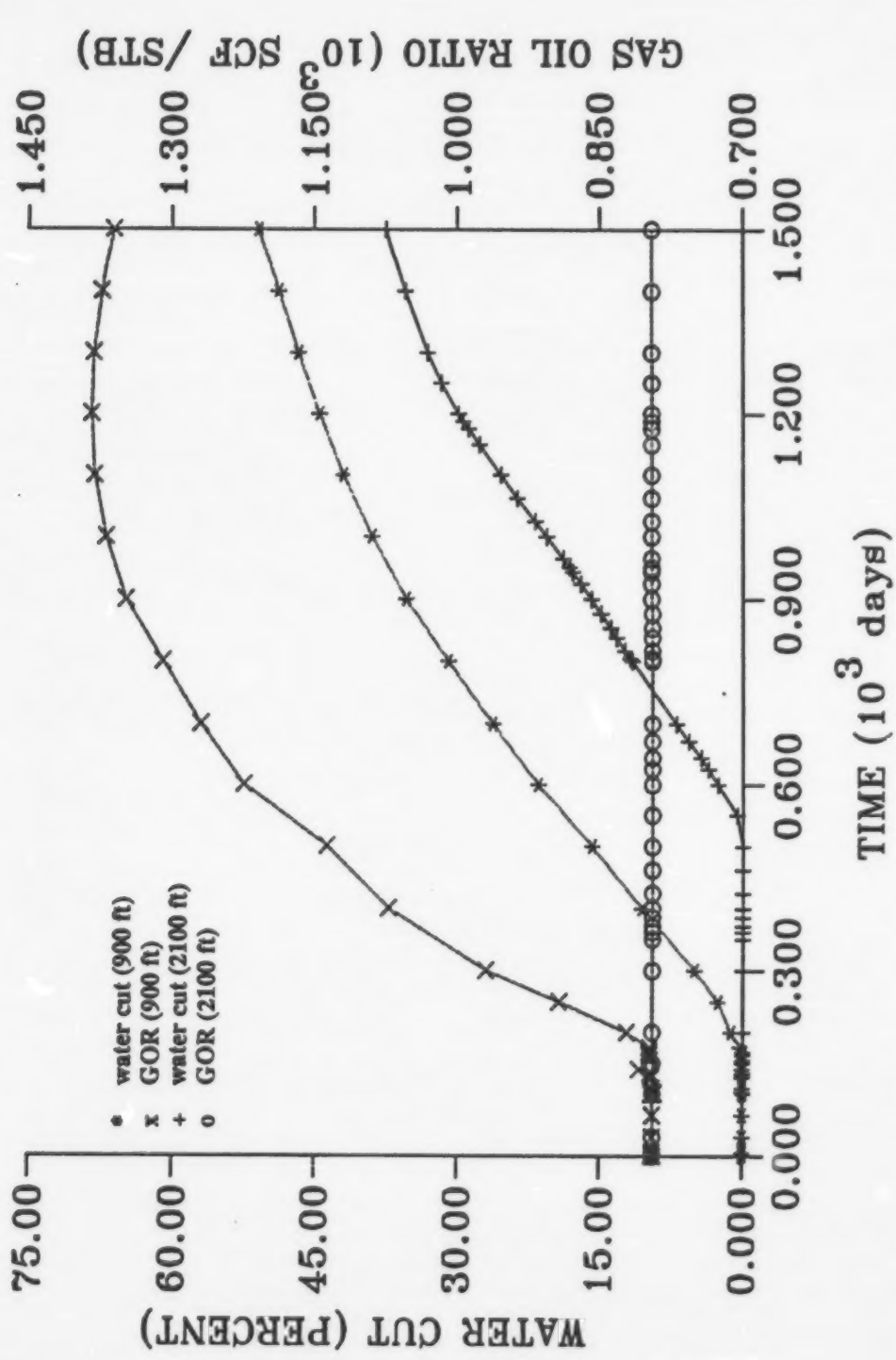

Figure 5: Water Cut and GOR Behavior for Horizontal Wells of Length 900 ft and 2100 ft with Liquid Rates of 3,000 Stb/day

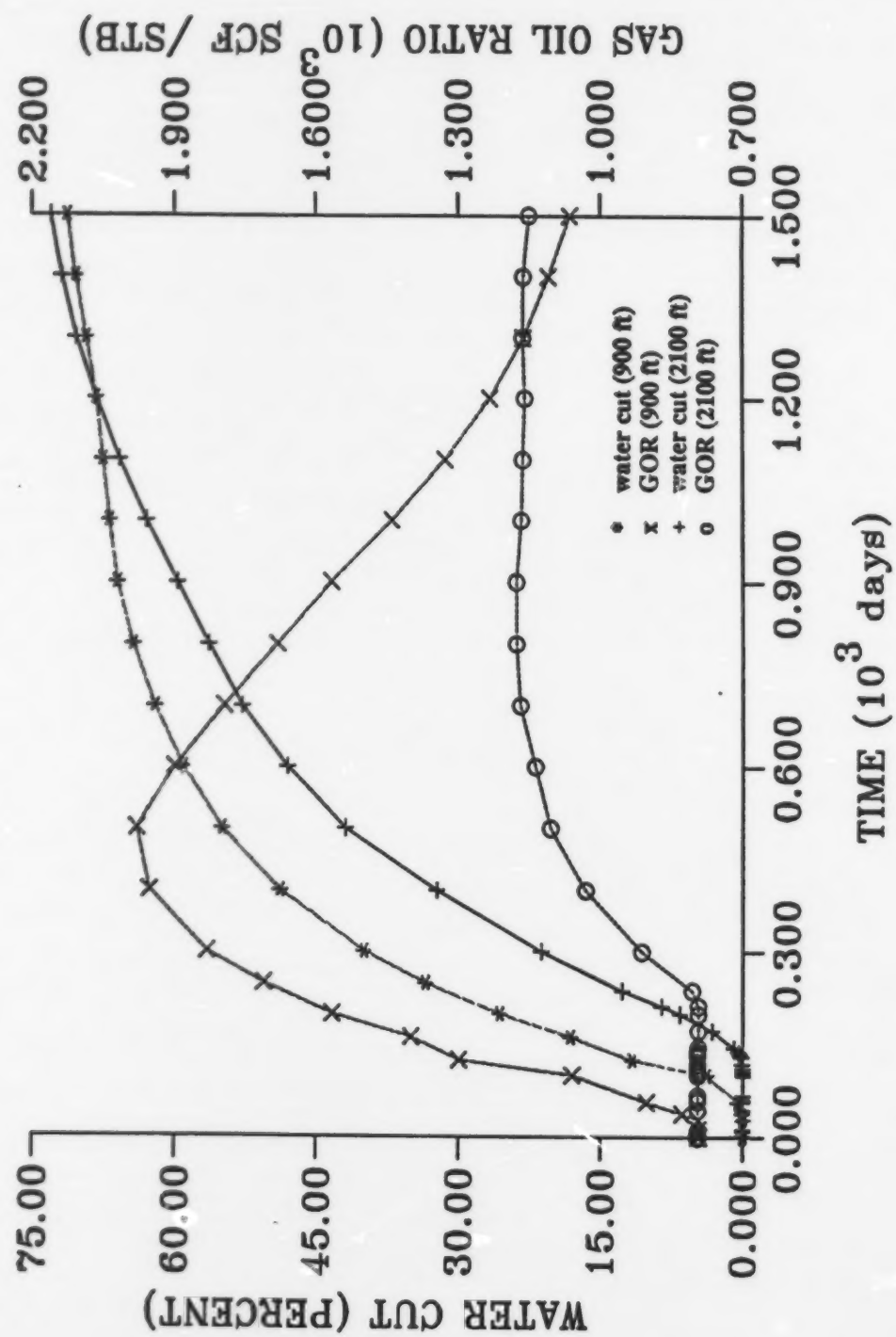

Figure 6: Water Cut and GOR Behavior for Horizontal Wells of Length 900 ft and 2100 ft with Liquid Rates of 6,000 Stb/day

Figure 7: Oil Production Rates and Cumulative Oil Produced for Horizontal Wells of Length 900 ft and 2100 ft with Liquid Rates of 3,000 Stb/day

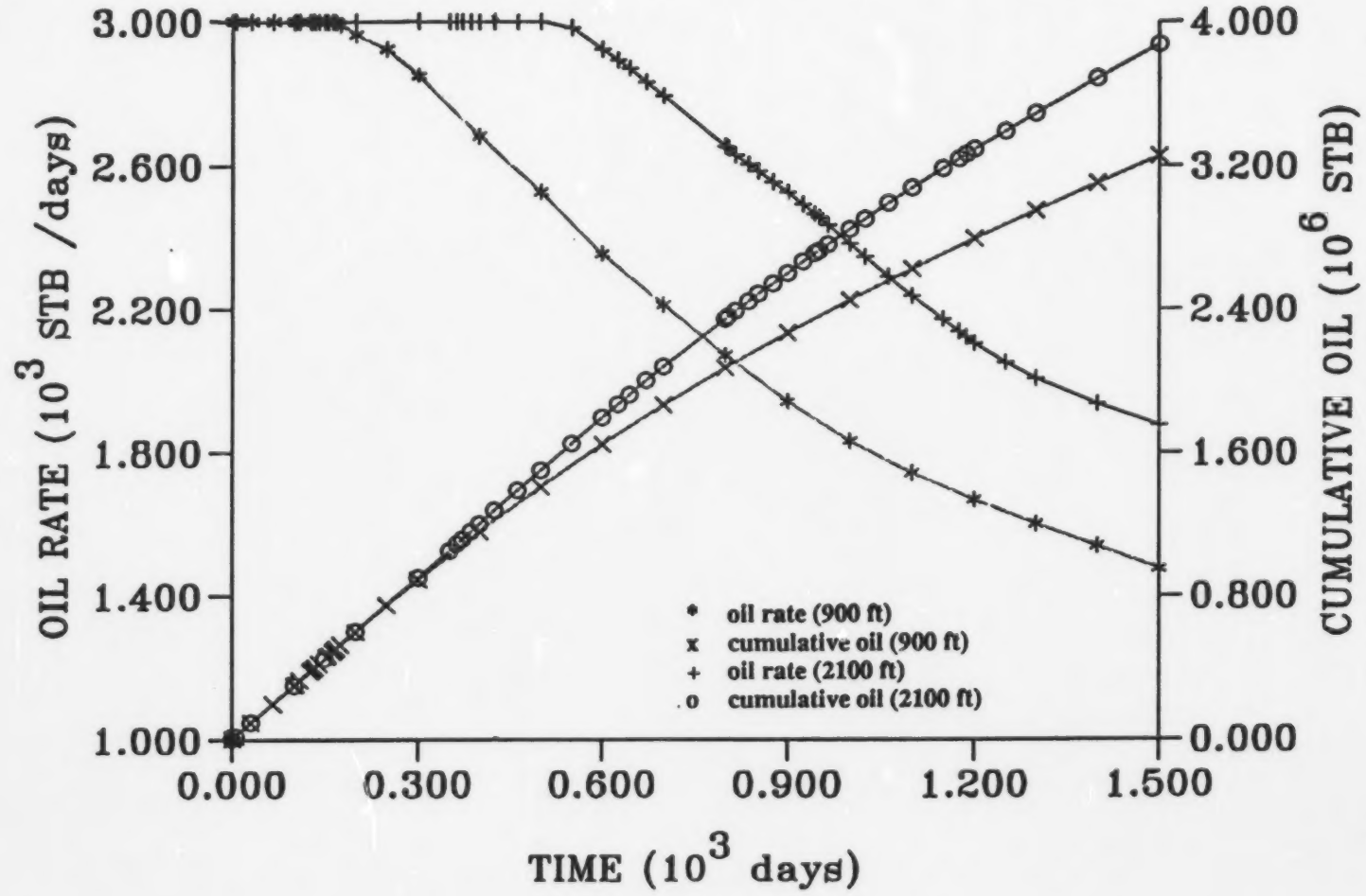

Figure 8: Oil Production Rates and Cumulative Oil Produced for Horizontal Wells of Length 900 ft and 2100 ft with Liquid Rates of 6,000 Stb/day

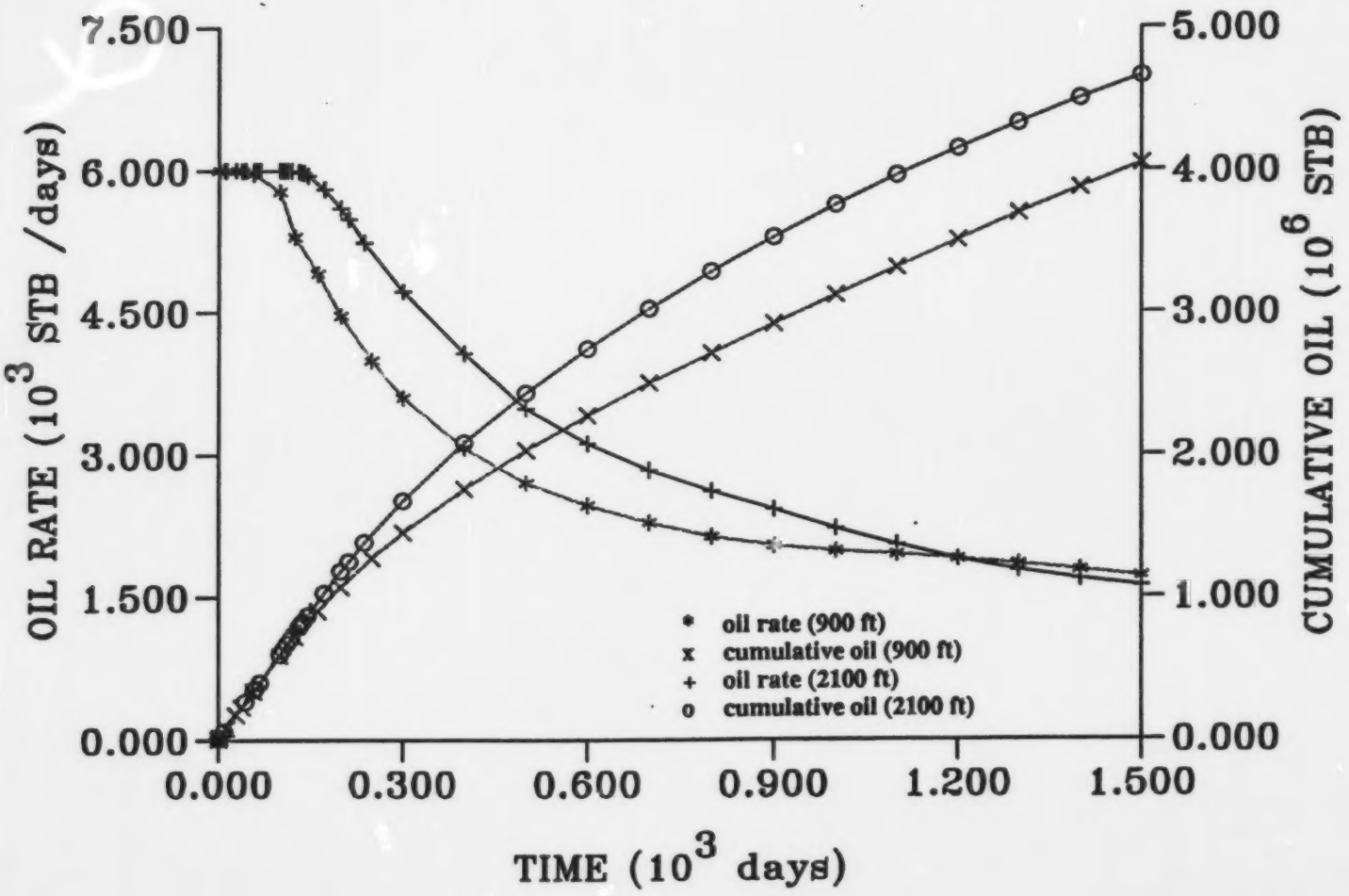

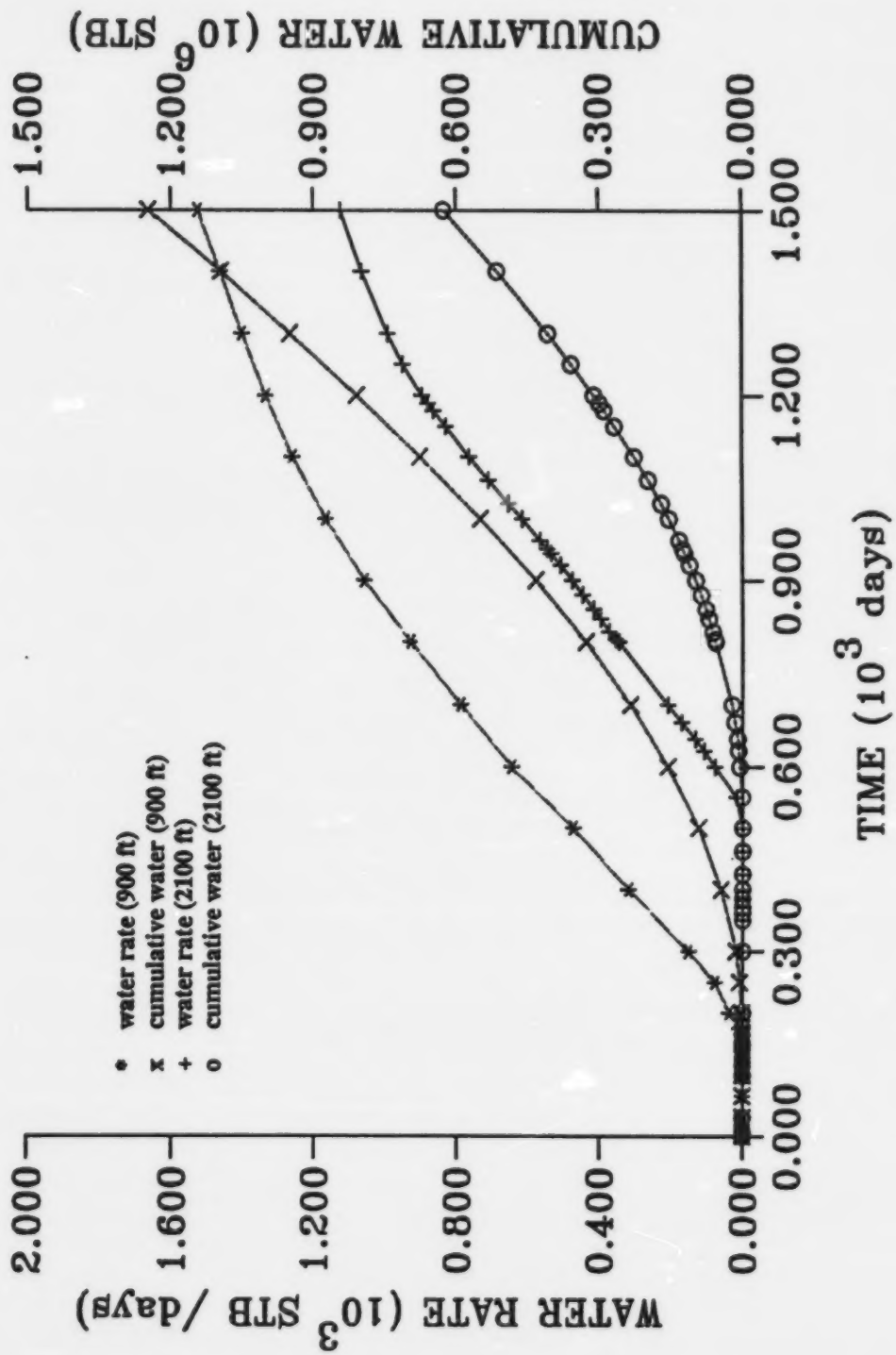

Figure 9: Water Production Rates and Cumulative Water Produced for Horizontal Wells of Length 900 ft and 2100 ft with Liquid Rates of 3,000 Stb/day

Figure 10: Water Production Rates and Cumulative Water Produced for Horizontal Wells of Length 900 ft and 2100 ft with Liquid Rates of 6,000 Stb/day

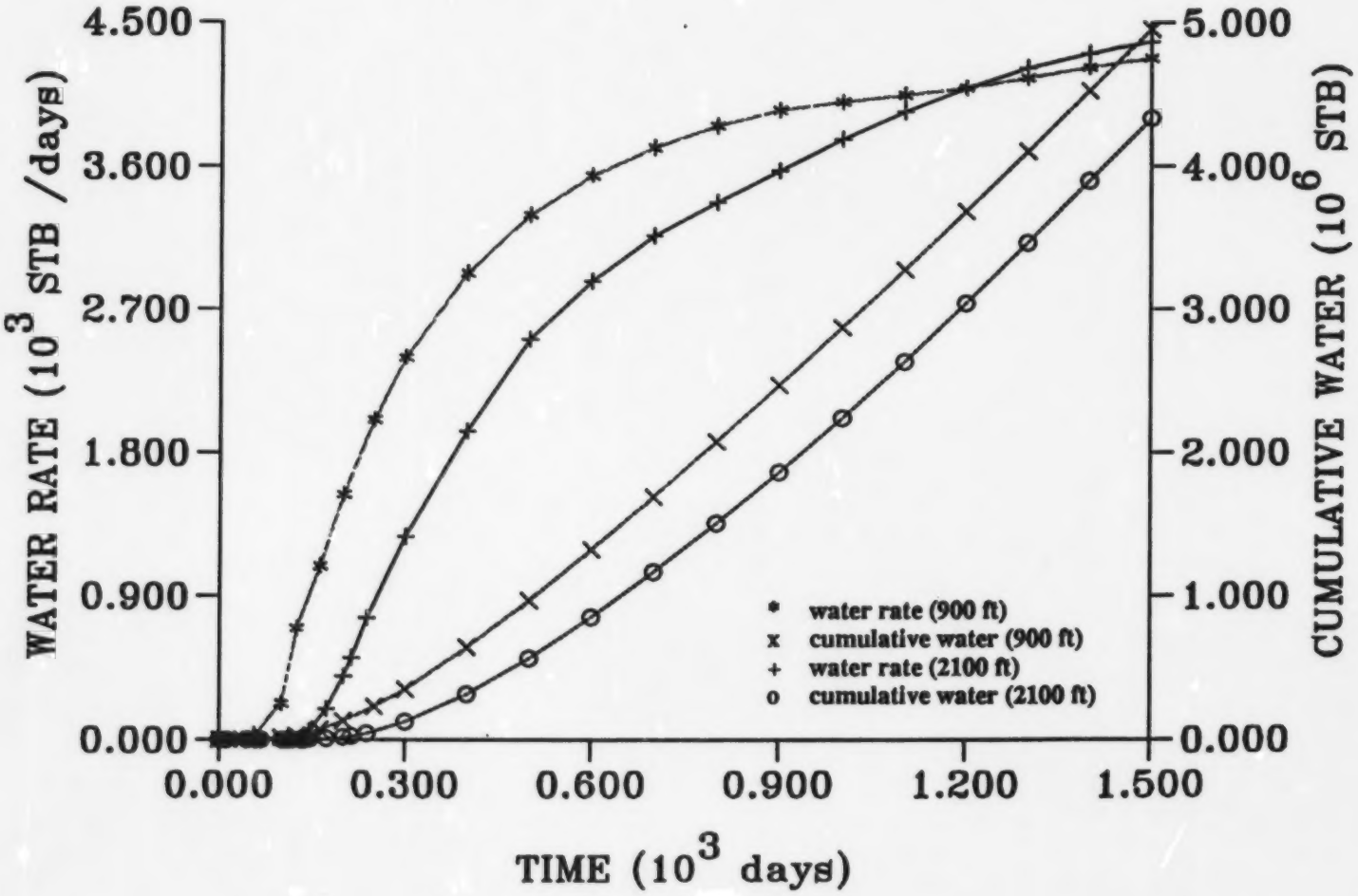

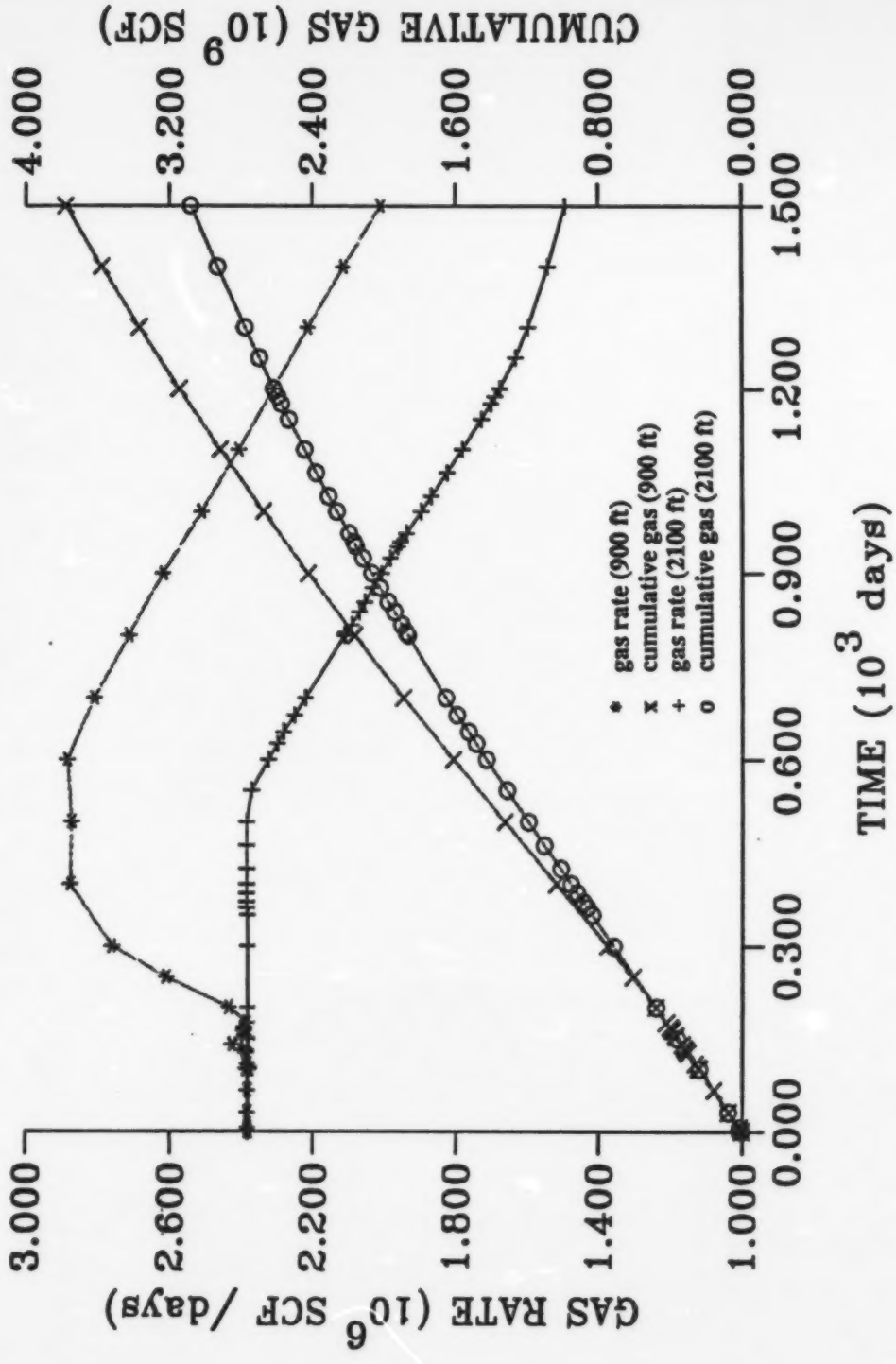

Figure 11: Gas Production Rates and Cumulative Gas Produced for Horizontal Wells of Length 900 ft and 2100 ft with Liquid Rates of 3,000 Stb/day

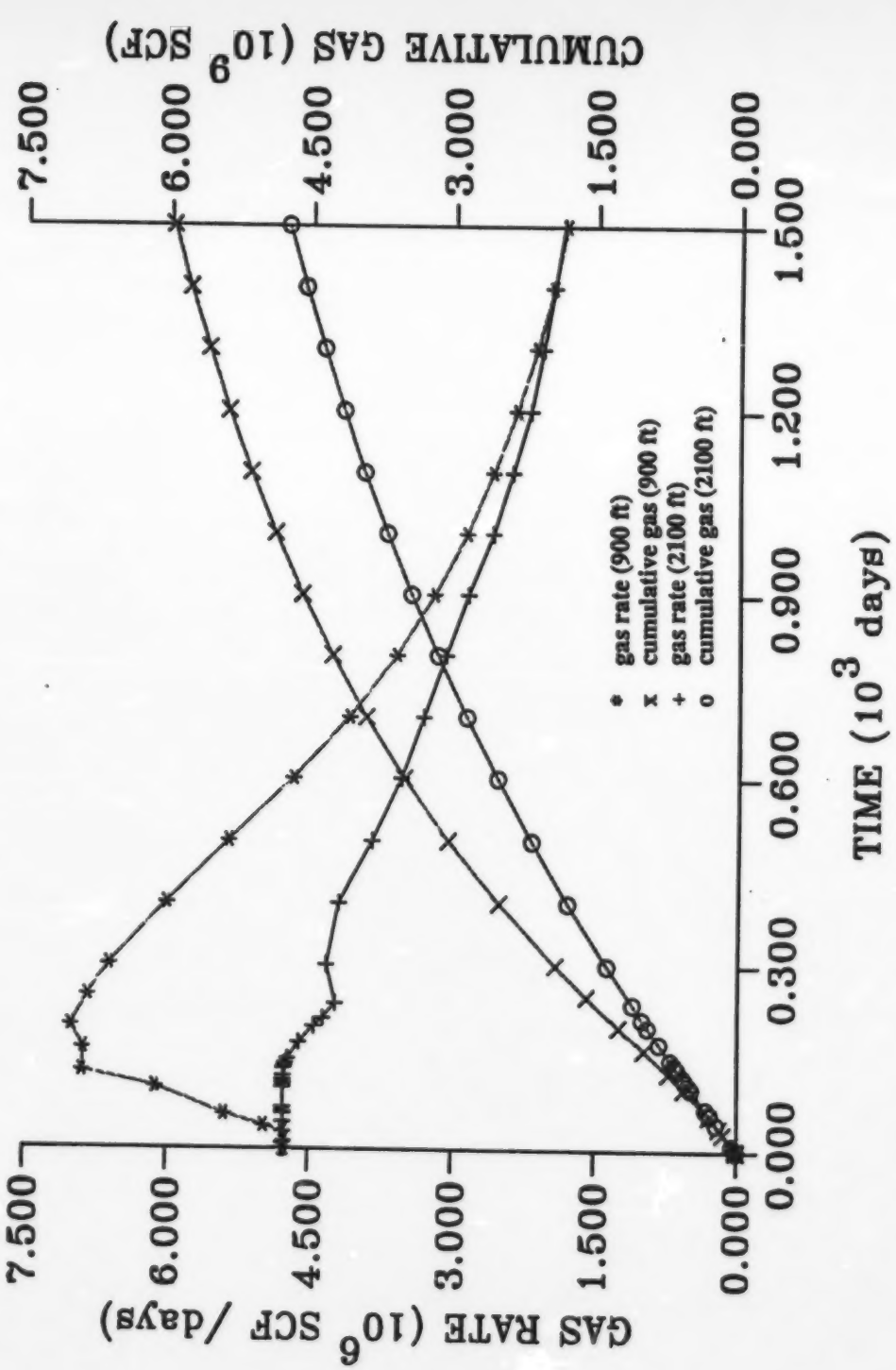

Figure 12: Gas Production Rates and Cumulative Gas Produced for Horizontal Wells of Length 900 ft and 2100 ft with Liquid Rates of 6,000 Stb/day

Figure 13: Variation of the Parameter α, the In Situ Gas Saturation (S_g) and the Correlation Predicted Gas Holdup (E_g) for the Wellblock Located in Gridblock (8,5,4). The Horizontal Well Length is 900 ft with a Liquid Rate of 6,000 Stb/day

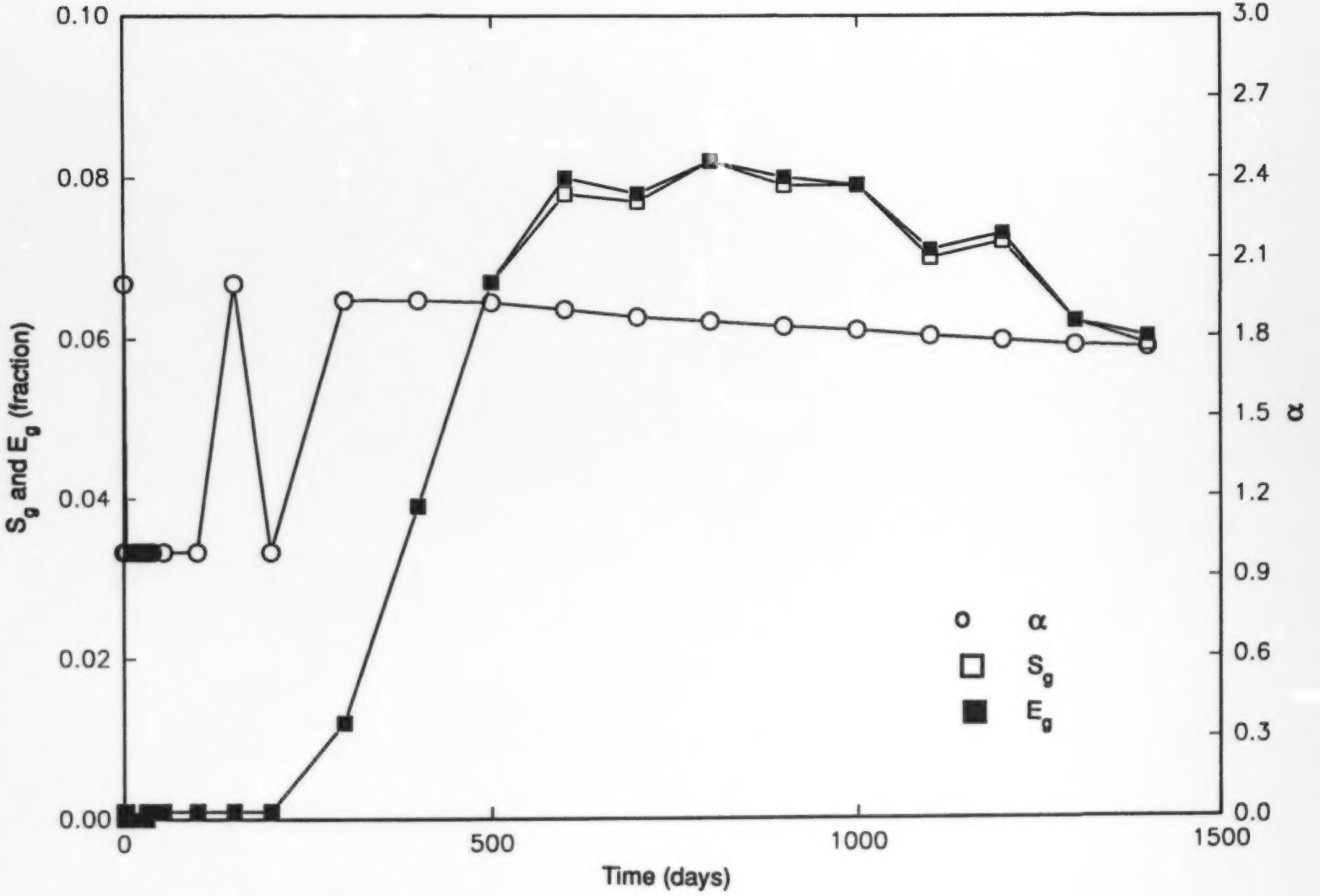

Figure 14: Comparison of Water Cut and GOR for a Horizontal Well (Length = 2100 ft and Liquid Rate = 6,000 Stb/day) Modelled with No Grid Refinement and Using Hybrid Grid Refinement (4 Radial, 4 Tangential)

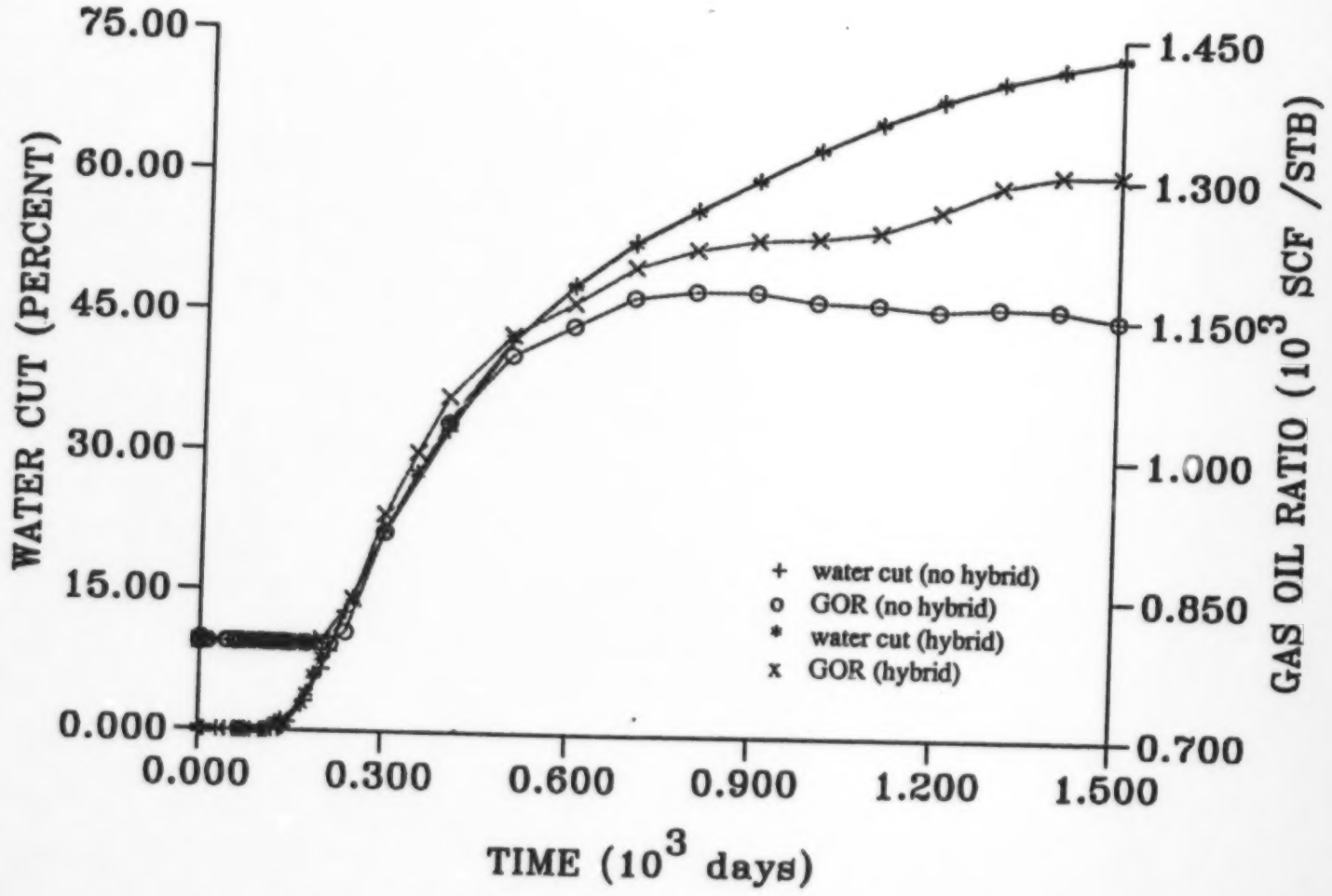

Figure 15: Predicted GOR for a Horizontal Well Modelled Using Different Levels of Hybrid Grid Refinement (Length = 2100 ft and Liquid Rate = 6,000 Stb/day)

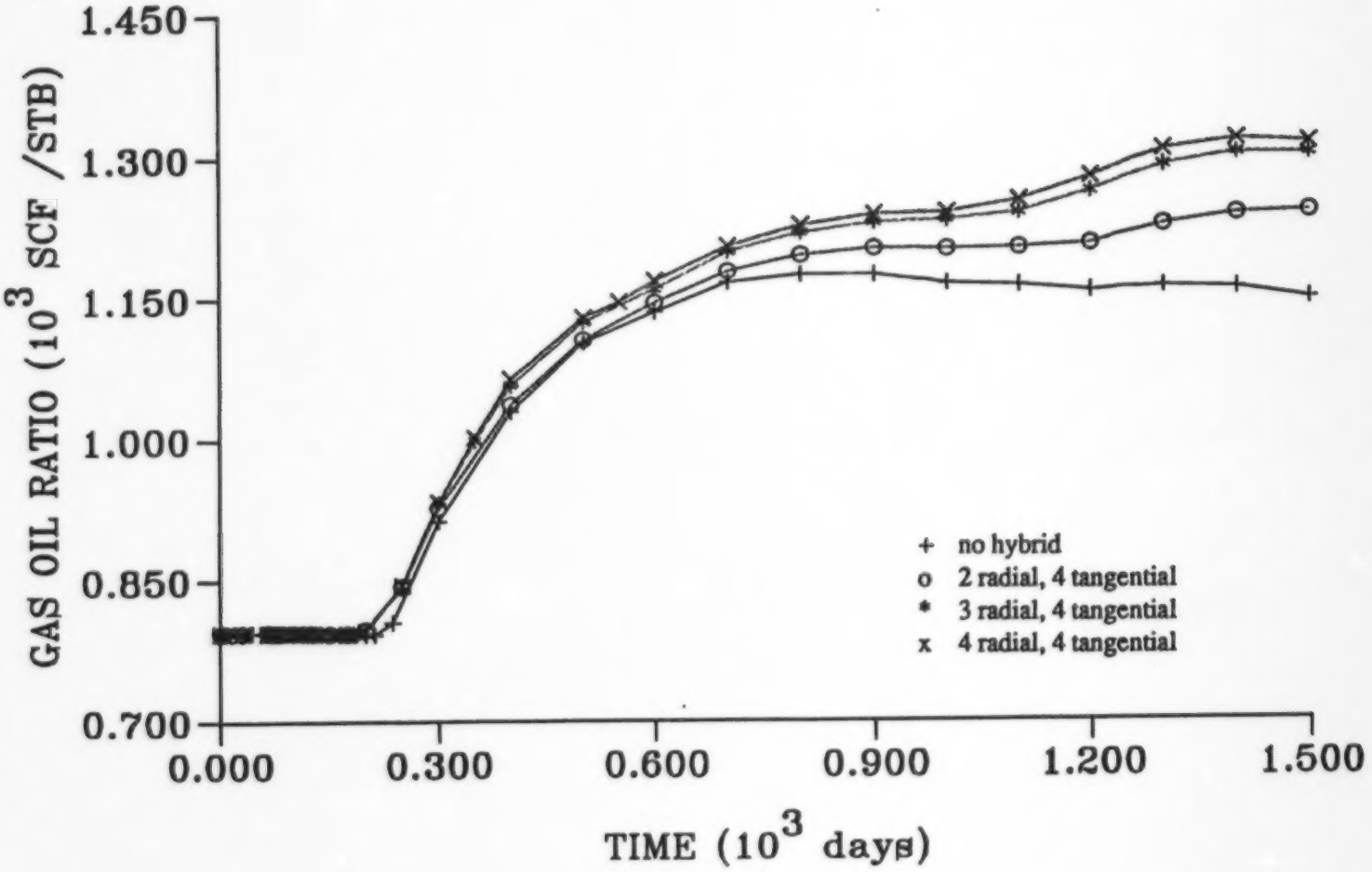

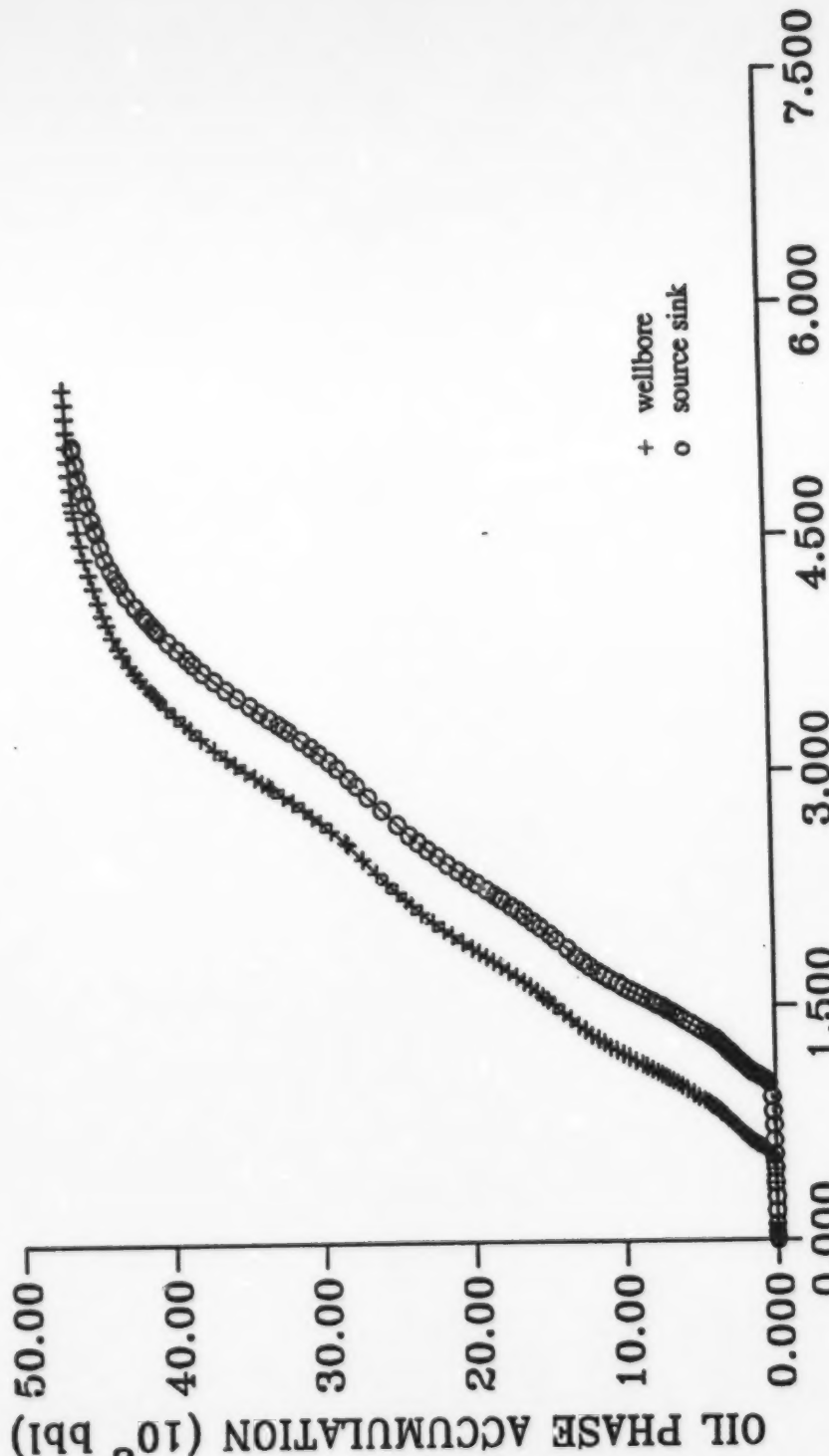

Figure 16: A Comparison of Cumulative Oil Production Predictions Using Traditional Source/Sink vs. New Wellbore Model for a Thermal, Dual Horizontal Well, Gravity Drainage Example

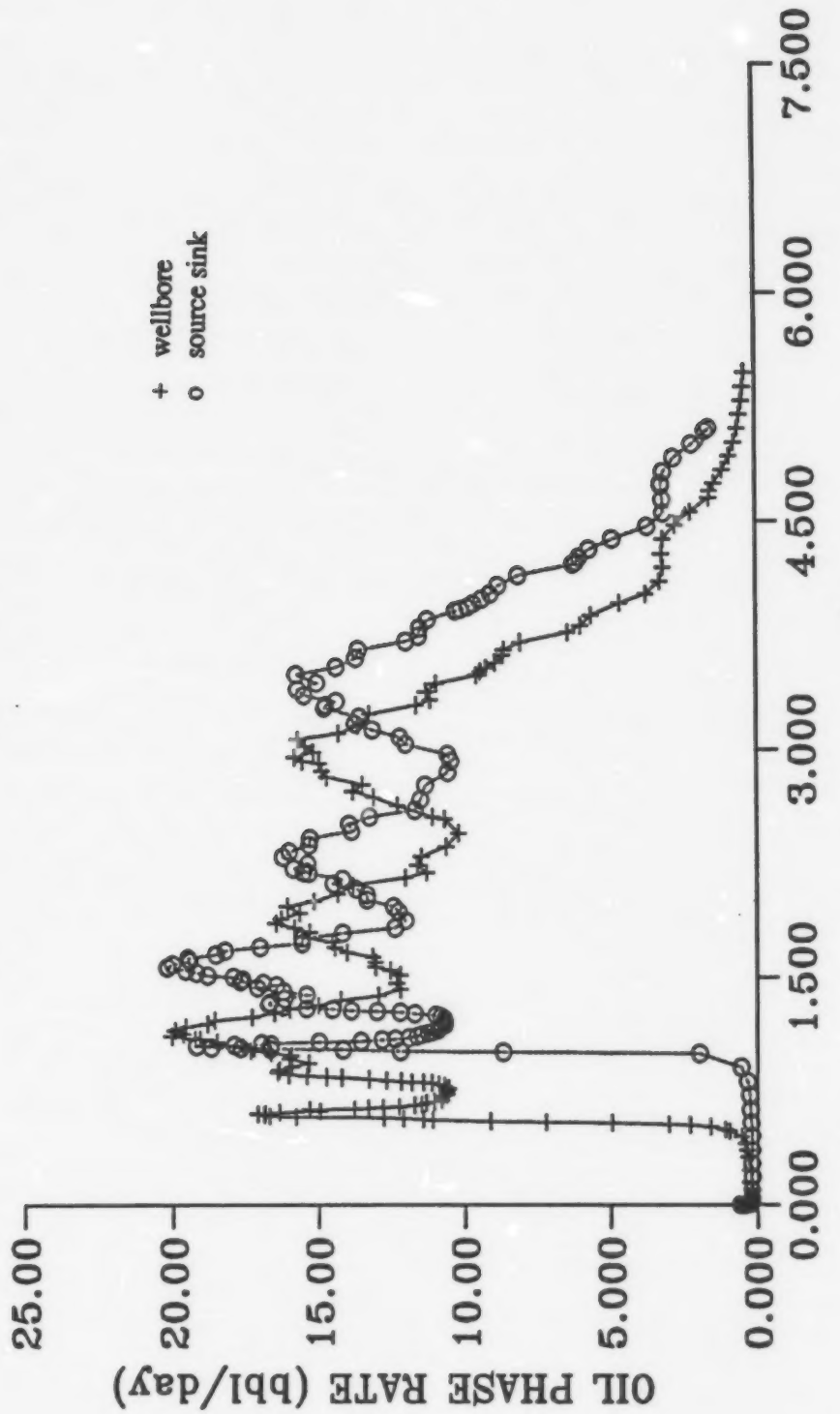

Figure 17: A Comparison of Instantaneous Oil Production Predictions Using Traditional Source/Sink vs. New Wellbore Model for a Thermal, Dual Horizontal Well, Gravity Drainage Example

Figure 18: Gas Saturation Profile (Vertical y-z Cross Section, I=1) After 1825 Days, Showing Tangential (Slope) Growth of the Steam Chamber